

Cite this: *Biomater. Sci.*, 2026, **14**, 780

# Beyond polydopamine: expanding the horizon of polycatecholamines for biomaterials and biomedical technologies

Elena Rainone, <sup>a,b</sup> Hossam Alshaiba <sup>a</sup> and Fabio Variola <sup>\*a,b,c,d</sup>

Polydopamine (pDA) has emerged as a benchmark material in bioinspired engineering, owing to its facile synthesis, strong adhesion, and chemical versatility. However, pDA is just one member of the broader polycatecholamine family, which includes poly-L-DOPA (pLD), polynorepinephrine (pNE), and polyepinephrine (pEP); each offering unique chemical functionalities and biological advantages. In this perspective, we critically assess the biomedical potential of these underexplored polymers, highlighting how their distinct physicochemical properties can expand current applications in surface modifications, coatings, biointerfaces, bioadhesives, biosensors, and carriers for drug delivery. Comparative analysis reveals that while pDA dominates the field, alternative polycatecholamines also exhibit equally attractive properties, such as enhanced hydrophilicity, biofunctionalization capacity, redox behaviour, and stimuli responsiveness. By broadening the focus beyond pDA, this work aims at catalysing future research on structurally diverse polycatecholamines as next-generation multifunctional biomaterials.

Received 8th September 2025,  
Accepted 10th December 2025

DOI: 10.1039/d5bm01357g

rsc.li/biomaterials-science

## Introduction

In the past two decades, the use of bioinspired materials has emerged as a transformative approach in biomedical engineering, offering innovative solutions that mimic strategies and mechanisms of living organisms. From the hierarchical structure of bone to the remarkable elasticity of skin, nature provides a rich template for developing materials with tailored mechanical, chemical, and biological properties.<sup>1</sup> Among these natural systems, marine organisms have attracted particular attention, especially in the context of surface adhesion. Underwater adhesion, long considered a significant challenge for synthetic materials, is efficiently achieved by marine mussels through specialized proteins known as mussel foot proteins (Mfps). Such proteins permit these mollusks to anchor themselves to a wide variety of wet surfaces, including rocks, wood, and metal, through complex interfacial interactions.<sup>2</sup> This extraordinary performance is largely attributed to the presence of the catecholic amino acid L-3,4-dihydroxyphenylalanine (L-DOPA), which is heavily concentrated in

specific Mfps such as Mfp-3 and Mfp-5.<sup>3</sup> The catechol side chain in L-DOPA plays a central role in adhesion by competitively binding to substrate surfaces and displacing interfacial water molecules, thereby promoting strong surface interactions under wet conditions.<sup>3</sup> These catechol groups establish a variety of reversible and irreversible interactions, including  $\pi$ - $\pi$  stacking, hydrogen bonding, van der Waals forces, hydrophobic interactions, coordination bonds with metal ions, and other electrostatic interactions.<sup>2-4</sup>

Despite the remarkable adhesive properties of Mfps, their practical use in biomedical applications has been limited by challenges related to large-scale extraction, purification, and stability.<sup>2</sup> To overcome these limitations, Lee *et al.* introduced a minimalist synthetic strategy by focusing on one of the key functional motifs of Mfps: the catecholamine structure of dopamine. They demonstrated that dopamine could spontaneously oxidize and polymerize in mildly alkaline aqueous solutions (pH  $\approx$  8.5), forming a thin, surface-adherent polydopamine (pDA) film on virtually any substrate.<sup>5</sup> This simple, one-step deposition technique offered a universal surface coating strategy, enabling facile functionalization of metals, polymers, ceramics, and biological materials. Since its introduction, pDA has rapidly emerged as an important material for the development of a wide array of biomedical applications, ranging from bioadhesives<sup>6</sup> and drug delivery systems<sup>7</sup> to biosensors,<sup>8</sup> among others. This is due to its biocompatibility, adhesive strength, redox activity, and chemical versatility.<sup>2,3,9</sup>

Dopamine is just one member of a broader family of endogenous catecholamines, which also includes norepi-

<sup>a</sup>Faculty of Engineering, Department of Mechanical Engineering, University of Ottawa, Ottawa, ON, Canada. E-mail: erain074@uottawa.ca, halsh081@uottawa.ca

<sup>b</sup>Ottawa-Carleton Institute for Biomedical Engineering, Ottawa, Canada

<sup>c</sup>Faculty of Medicine, Department of Cellular and Molecular Medicine, University of Ottawa, Ottawa, ON, Canada

<sup>d</sup>Children's Hospital of Eastern Ontario (CHEO), Ottawa, ON, Canada. E-mail: fabio.variola@uottawa.ca



nephrine, epinephrine, and L-DOPA. These molecules all share a common chemical structure composed of a catechol ring (*i.e.*, a benzene ring with two adjacent hydroxyl groups) and an amine-containing side chain, which allows for both redox activity and surface reactivity.<sup>10,11</sup> This is illustrated in Fig. 1A, which displays the biosynthetic pathway of catecholamines starting from the amino acid tyrosine. Importantly, tyrosine itself lacks a catechol moiety and is therefore not classified as a catecholamine. Conversely, its downstream products (L-DOPA, dopamine, norepinephrine, and epinephrine) acquire catechol functionality through enzymatic hydroxylation.

Beyond their shared chemistry, these catecholamines exert distinct yet interconnected physiological functions. Acting as both neurotransmitters and hormones, they translate their molecular reactivity into complex biological signaling.<sup>10,12,13</sup> Specifically, when synthesized in the brain, dopamine regulates movement, emotional reactions, learning, and memory.<sup>14</sup> In the cardiovascular system, its effects are dose-dependent; lower concentrations dilate renal and coronary arteries to improve perfusion, while high concentrations stimulate  $\beta$ -receptors to increase cardiac output; excessive doses may instead trigger vasoconstriction and hypertension.<sup>13</sup> Epinephrine increases heart rate and blood pressure, promotes skeletal muscle vasodilation, and modulates glucose metabolism and apprehensive/passive emotional expression.<sup>13,15,16</sup> Norepinephrine, conversely, induces systemic vasoconstriction, activates baroreceptors to reduce heart rate, and is linked to active, aggressive emotional expression.<sup>13,16</sup> Importantly, beyond their physiological significance, these molecules have

long-standing pharmacological and clinical use. For example, norepinephrine and epinephrine have been used for decades as vasoactive agents in circulatory support,<sup>17</sup> with the latter being widely known for its role in treating anaphylaxis *via* the EpiPen®. Likewise, L-DOPA remains a cornerstone in the treatment of Parkinson's disease.<sup>18</sup>

Given their physiological roles, chemical similarity to dopamine, and availability as pharmaceutical compounds, these alternative catecholamines are equally attractive candidates for the design of functional (bio)materials. In fact, polymerization studies on these molecules began shortly after the introduction of pDA. Polynorepinephrine (pNE), for instance, was first reported in 2009.<sup>19</sup> Yet, despite this early start, alternative catecholamine-based polymers have received disproportionately little attention. In 2022, nearly 2,000 publications referenced pDA (Fig. 1B), while only a handful explored poly-L-DOPA (pLD), pNE, or polyepinephrine (pEP) (Fig. 1C). This disparity reveals a significantly overlooked research potential, especially when considering the shared catecholamine-derived functionalities, biomedical relevance, and additional promising properties of these materials.

To contribute to bridge this gap, this perspective aims to critically examine these lesser-studied materials by analyzing four major biomedical applications: surface modifications, bioadhesive technologies, biosensors, and drug delivery systems. Our main goal is to broaden the current focus beyond polydopamine-based polymers and foster a more diverse exploration of polycatecholamine systems. By shedding light on their unique properties, challenges, and emerging opportu-

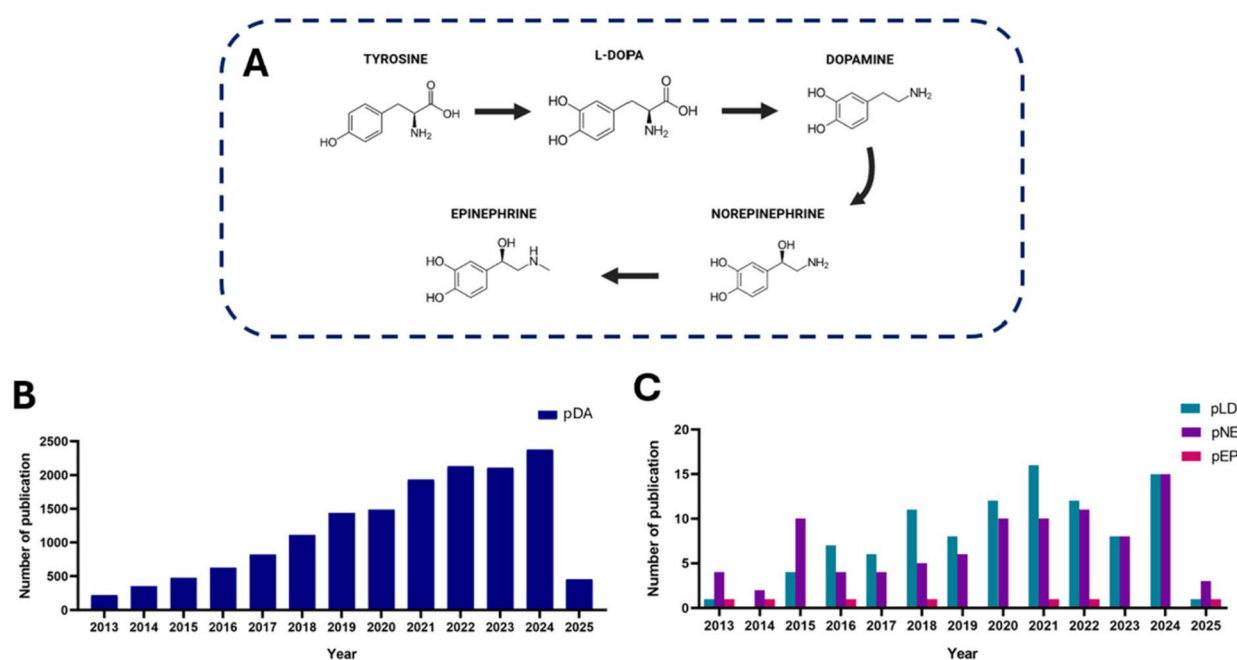


**Fig. 1** (A) Biosynthetic pathway of catecholamines showing the enzymatic conversion of tyrosine to L-DOPA, dopamine, norepinephrine, and epinephrine. These molecules share a catechol moiety and serve as precursors for the corresponding polycatecholamine coatings. Number of publications sorted by year in terms of (B) polydopamine (pDA), (C) poly-L-DOPA (pLD), polynorepinephrine (pNE), and polyepinephrine (pEP). Data were collected from the "Web of Science" (15<sup>th</sup> March 2025).



nities, the objective of this perspective is to catalyze future research efforts that could lead to impactful advancements in the biomedical field.

## Polycatecholamines

Since its introduction in 2007, pDA has become a benchmark material in bioinspired surface science due to its versatility, ease of deposition, and adhesive performance.<sup>5</sup> It is the most widely studied polycatecholamine and the reference for comparing newer analogues. Polynorepinephrine, the first catecholamine polymer reported after pDA in 2009,<sup>19</sup> arises from norepinephrine, which differs from dopamine by an extra hydroxyl group on its alkyl chain. This functionality has been used to enable distinct post-modification chemistries compared with pDA, including surface initiated ring opening polymerization,<sup>19</sup> enabling the growth of biodegradable polymers directly from the pNE coating. Polypinephrine derives from epinephrine, which (relative to dopamine) carries both a  $\beta$ -hydroxyl and an *N*-methyl (secondary) amine. These features influence polymerization behaviour, resulting in lower reactivity and typically less stable coatings compared to pDA<sup>11</sup> which may be useful for temporary or regenerable coatings where controlled removal is desirable. Lastly, another polycatecholamine that is emerging as a promising alternative is poly-L-DOPA. Structurally, L-DOPA differs from dopamine by the presence of an additional carboxylic acid group. This group is retained even after the polymerization<sup>20</sup> providing additional handles for conjugation,<sup>20,21</sup> and tuning interfacial charge,<sup>22</sup> offering a functional edge over pDA. Moreover, the presence of the carboxylic group in L-DOPA establishes an  $\alpha$ -carbon, making the molecule inherently chiral, a feature that is absent in dopamine. This chirality, coupled with the carboxylate's supramolecular interaction potential, enables advanced templating strategies that are not intrinsically available to dopamine-based systems.<sup>23</sup> This introduces a new dimension to pLD, with possible applications in chirality-responsive interfaces and enantioselective biomolecular interactions. Together, these side-chain differences modulate redox behavior, morphology, and surface properties, features that define performance across surface modification, bioadhesion, biosensing, and drug delivery. The comparative analysis is discussed in the sections below.

## Polymerization mechanisms

Polycatecholamines are typically synthesized *via* the self-polymerization of their precursor in mildly alkaline aqueous solutions (pH  $\approx$  8.5), conditions that mimic the marine environment in which mussel adhesion occurs.<sup>5,19,24,25</sup> Alternative coating strategies have also been developed for all polycatecholamines, including electropolymerization,<sup>26–30</sup> and enzymatic oxidation.<sup>31–35</sup> In electropolymerization, an applied potential drives the monomer oxidation at the electrode

surface, enabling spatially controlled deposition on conductive substrate, a feature particularly suited for biosensors application.<sup>26</sup> The success of electropolymerization depends on a combination of monomer oxidation state, electrode material, and scan rate. This is particularly critical for pEP, where the secondary amine can hinder film formation.<sup>36</sup> Nevertheless, adherent polyepinephrine coatings have been successfully generated on glassy carbon electrodes by employing pre-oxidation, fast voltammetry, or neutral pH conditions.<sup>29,30</sup> On the other hand, the enzymatic oxidation uses enzymes such as laccase,<sup>35</sup> horseradish peroxidase,<sup>33</sup> tyrosinase<sup>32</sup> to catalyze the monomer. This oxidation under milder and more biocompatible conditions, making it suitable for cell-interfacing materials and tissue engineering.<sup>31</sup> Under these conditions, each catecholamine undergoes oxidation to reactive intermediates, which subsequently triggers intramolecular or intermolecular cyclizations characteristic of their specific structure.

Despite the ongoing debates about pDA formation pathways,<sup>39</sup> it is widely recognised that the first step consists of the oxidation of dopamine to dopamine-quinone, followed by an intramolecular cyclization to form 5,6-dihydroxyindole (DHI), a key intermediate in pDA formation,<sup>37,40–42</sup> Fig. 2A. For pNE and pLD, the first step is similar, but their different side chains also effect the intermediates formed.

Notably, tautomerization and oxidative cleavage of the  $\beta$ -hydroxyl-bearing side chain in norepinephrine generate 3,4-dihydroxybenzaldehyde (DHBA), which can undergo Schiff base condensation with the amine group of another norepinephrine molecule (Fig. 2C).<sup>38</sup> Upon reduction, this leads to the formation of DHBA-NE intermediates, which are proposed to contribute to unique interunit linkages within the polymer network.<sup>38</sup> These include hydroxyethylaminomethyl bridges between catechol units; structural features that are absent in pDA.<sup>24,38</sup> As a result, polynorepinephrine exhibits a slower growth kinetics, reduced aggregation tendency, and distinct physical properties. Compared to pDA, pNE tends to form structures with significantly smoother and thinner morphologies, a phenomenon also observed when DHBA is added exogenously to dopamine polymerization systems.<sup>38,43</sup>

In contrast, the carboxyl group on L-DOPA leads to the formation of 5,6-dihydroxyindole-2-carboxylic acid (DHICA), which together with DHI are the same key intermediates of natural eumelanin (Fig. 2B).<sup>22,24,44</sup> This carboxylic group introduces electrostatic repulsion and steric hindrance, which slows polymerization kinetics and hinders surface deposition, particularly under standard alkaline buffer conditions.<sup>20,45</sup> To address these limitations, several environmental parameters, commonly used in catecholamine polymerization, have also been applied to optimize pLD formation. These include ionic strength, which screens carboxylate repulsion;<sup>20</sup> temperature, which accelerates oxidation kinetics;<sup>46</sup> and the use of chemical oxidants such as NaIO<sub>4</sub>, which enhance deposition rate.<sup>47</sup>

Unlike the other polycatecholamines, pEP follows a distinct oxidative route that bypasses the formation of DHI. Instead, during alkaline autooxidation, epinephrine first forms adrenochrome, which then rearranges into adrenolutin, a fluorescent



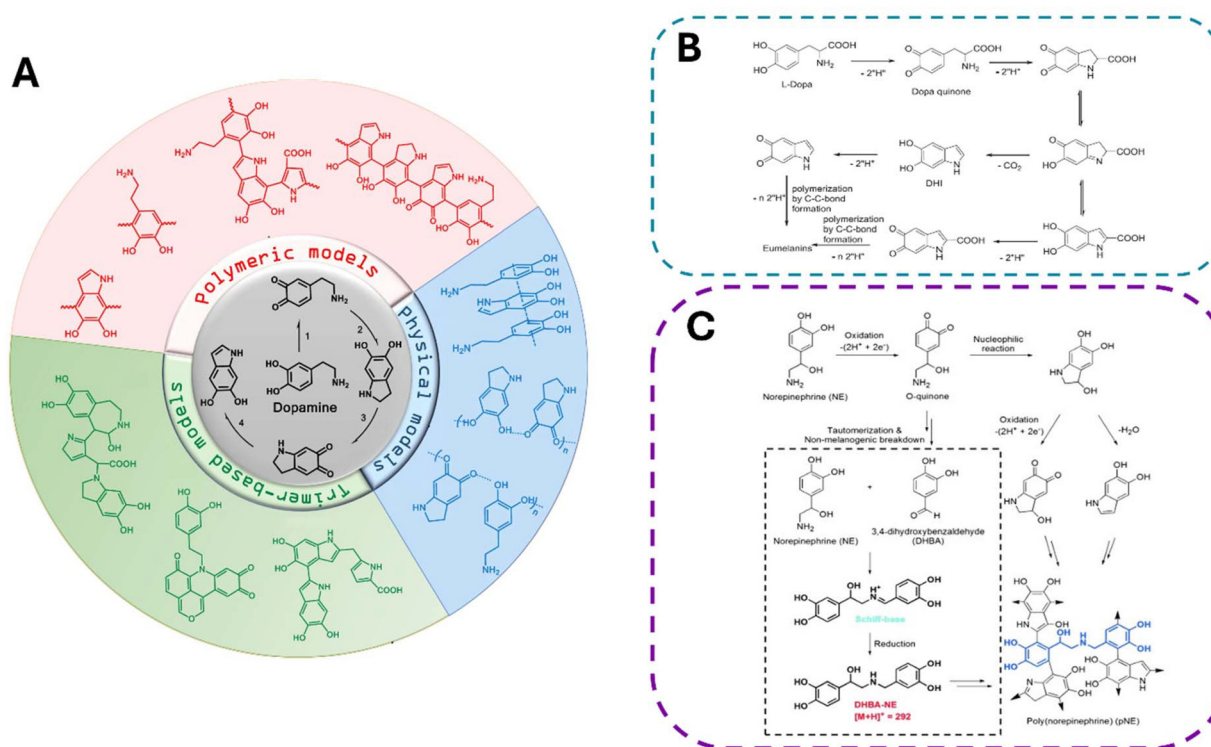


**Fig. 2** (A) The widely accepted mechanism of dopamine auto-oxidation leading to the formation of polydopamine building blocks with the three major structural models proposed for polydopamine assembly. Readapted from ref. 37 licensed under CC BY 4.0 (<https://creativecommons.org/licenses/by/4.0/>). (B) Oxidative polymerization of L-DOPA leading to the formation of eumelanins. Reprinted with permission from ref. 24. Copyright 2019 Wiley. (C) Proposed oxidation and polymerization pathway of polynorepinephrine. Adapted with permission from ref. 38. Copyright 2013 Wiley.

indole derivative bearing a 3-hydroxyl group.<sup>25,48,49</sup> This transformation occurs *via* rapid internal cyclization. Bacil *et al.* quantified this step at a rate of  $18.9 \text{ s}^{-1}$ , nearly 80 times faster than the equivalent cyclization in dopamine ( $0.24 \text{ s}^{-1}$ ).<sup>50</sup> The heightened reactivity is attributed to the secondary amine in epinephrine, which acts as a stronger nucleophile than the primary amine of dopamine.<sup>49,50</sup> Interestingly, the polymerization of epinephrine under oxidative conditions has been studied for decades, though historically more in the context of aminochrome chemistry and its downstream rearrangement products.<sup>51,52</sup> Only recently has attention shifted toward epinephrine as a viable building block for functional polycatecholamine materials, with studies exploring its potential for self-assembly.<sup>25,35</sup>

A key challenge across all polycatecholamines is the partially understood nature of their final structure. This process depends strongly on multiple factors. As detailed in previous studies,<sup>11,31,53</sup> pDA formation *via* simple oxidation in solution is influenced by multiple factors, including dopamine concentration, buffer composition, pH, and the presence of exogenous oxidants. The resulting pDA structure is highly dependent on these parameters, which also dictate whether it deposits as a surface coating or forms particle/aggregate in suspension. The proposed structural models for pDA can be broadly categorized into polymeric,<sup>5,39,54</sup> physical aggregation-based,<sup>55,56</sup> and trimer-based models<sup>57</sup> (Fig. 2A). Each suggests different

degrees of chemical bonding and supramolecular organization, ranging from linear covalent polymers to non-covalent  $\pi$ - $\pi$  stacked assemblies. Similarly even its analogues likely undergoes self-assembly through a combination of covalent and non-covalent interactions, including  $\pi$ - $\pi$  stacking and cation- $\pi$  stabilization, which are central to the polymer growth and structural organization.<sup>23-25,58</sup> This self-assembly process is also highly environment dependent. For instance, the pEP self-polymerization pathway process has been shown to strongly depend on buffer environment (Tris, PBS, and NaOH) which influence both optical properties and the morphology of the aggregates.<sup>25</sup> However, compared to pDA, limited studies are available that systematically compare these aspects, and the possible different structures of the final polymers remain poorly characterized. The precise identity of monomer units, the presence of branching or crosslinking, and long-range structural organization are yet to be fully elucidated. This leaves a definite structural model even more elusive than for pDA.

## Biomedical applications

### Surface modifications

pDA is widely recognized for its role in biomaterials surface modification due to its excellent biocompatibility and cell



instructive properties. pDA's strong adhesiveness, largely due to its catechol groups,<sup>59</sup> coupled with the ability to significantly enhance the hydrophilicity of surfaces,<sup>5</sup> are crucial factors for biomedical applications such as coatings for biomedical implants and tissue engineering scaffolds.<sup>60</sup> Notably, pDA can increase the wettability of both hydrophobic and hydrophilic surfaces,<sup>5</sup> enhancing their functionality by introducing hydrophilic amino and hydroxyl groups that interact readily with water molecules, thus improving surface affinity for water.<sup>61,62</sup>

Building on this benchmark, pNE forms more uniform and smoother coatings compared to pDA, a feature that is attributed to the formation of the intermediate DHBA during polymerization.<sup>38</sup> Specifically, while pDA coatings can reach up to 100 nm in thickness and tend to form irregular aggregates (Fig. 3B), pNE layers remain ultrathin ( $\sim 12$  nm) and free of such surface roughness (Fig. 3B), ensuring excellent conformality and nanoscale uniformity.<sup>38</sup> Similarly, poly-L-DOPA coatings are also known to produce smoother and more uniform surfaces than pDA (Fig. 3A).<sup>22</sup> This difference is attributed to the presence of a carboxylic group in L-DOPA, which becomes deprotonated under alkaline conditions and enhances the solubility and dispersion of pLD oligomers in aqueous media.<sup>22</sup> As a result, pLD forms a structurally finer coating with reduced nanoscale roughness and improved con-

formality and enhanced physicochemical stability.<sup>22</sup> Unlike pDA films, which degrade under strongly acidic or basic conditions, pLD coatings maintain their integrity under a wider pH range (3–10).<sup>22</sup> Atomic Force Microscopy (AFM) studies have also confirmed that both pLD and pNE form smoother than pDA.<sup>28</sup>

These structural and chemical differences directly impact surface properties: pNE-coated materials exhibit superior hydrophilicity, with contact angles as low as  $8.7^\circ$  on silicon and  $22.9^\circ$  on gold, in contrast to  $31.2^\circ$  and  $34.1^\circ$  for pDA-treated substrates.<sup>38</sup> Likewise, pLD coatings further improve surface wettability as shown in Fig. 3C, yielding lower contact angles ( $29^\circ$ ) than both pDA ( $45^\circ$ ) and pNE ( $38^\circ$ ),<sup>63</sup> consistently enhancing the hydrophilicity of diverse substrates.<sup>46,64–66</sup> By contrast, pEP is less hydrophilic than pDA, a result of its methylated secondary amine, which reduces hydrogen bonding and results in higher water contact angles.<sup>35,67</sup> Nevertheless, it remains sufficiently hydrophilic to maintain aqueous dispersibility, supporting stable coating formation.<sup>35</sup>

From a biological viewpoint, variations in chemical structures translate into distinct cellular responses. In particular, pDA effectively immobilizes extracellular proteins, a factor that contributes to exhibit broad *in vitro* cytocompatibility across various cell types, including osteoblasts, neural and endothelial cells,<sup>68,69</sup> confirming its suitability as a cell-instructive

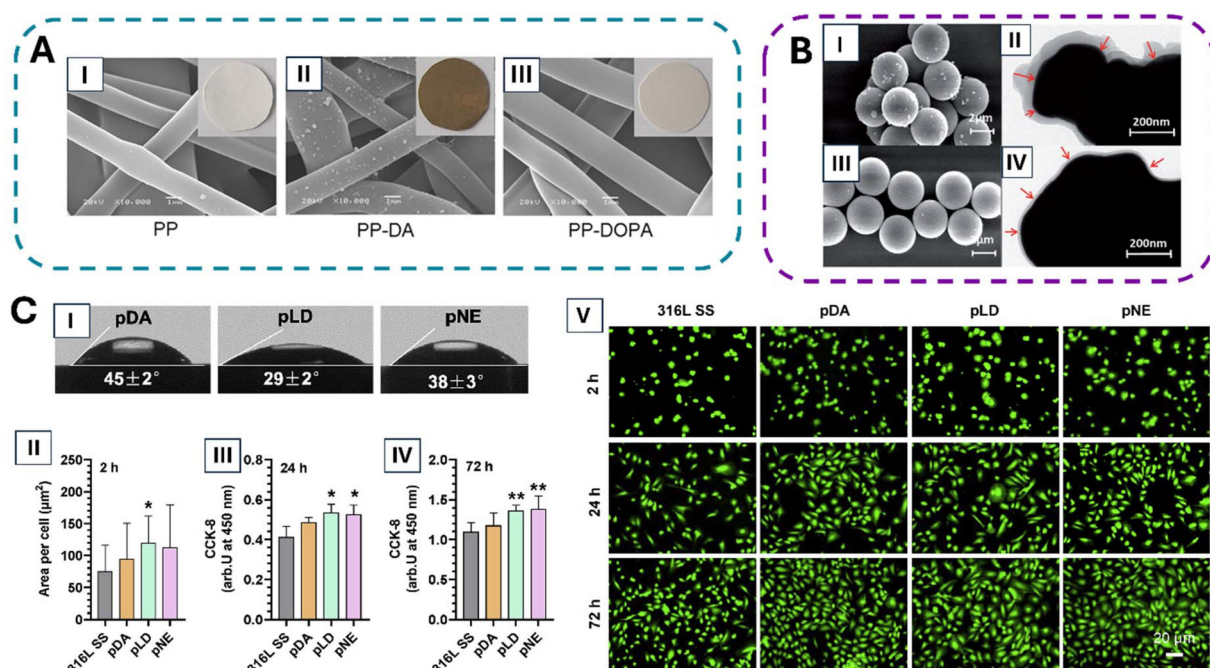


**Fig. 3** (A) SEM images (scale bar =  $1 \mu\text{m}$ ) of polypropylene (PP) membranes: (I) unmodified, (II) after polydopamine coating, and (III) after poly-L-DOPA modification. Adapted with permission from ref. 22. Copyright 2013 Elsevier. (B) (I) SEM image (scale bar =  $2 \mu\text{m}$ ) of polydopamine coating on polystyrene; (II) TEM image (scale bar =  $200 \text{ nm}$ ) of polydopamine coating on silver nanoparticles; (III) SEM and (IV) TEM images of polynorepinephrine coatings on the same substrates. Adapted with permission from ref. 38. Copyright 2013 Wiley. (C) (I) Static water contact angles of catecholamine-coated 316L stainless steel substrates. Adhesion/spreading of HUVECs cultured on bare 316L SS, pDA-, pLD-, and pNE-coated surfaces. (II) Cell-spread area per cell after 2 h. (III–IV) Cell proliferation after 24 h and 72 h, respectively, assessed by CCK-8 assay. \* $p < 0.05$ , \*\* $p < 0.01$  vs. bare 316L SS. (V) Fluorescence images of HUVECs cultured on the different surfaces for 2, 24, and 72 h. Scale bar =  $20 \mu\text{m}$ . Reproduced from ref. 63 licensed under CC BY-NC-ND 4.0 (<https://creativecommons.org/licenses/by-nc-nd/4.0/>).



interface. However, smoother and more conformal films tend to reduce nonspecific protein adsorption and promote more reproducible cell–material interactions, a desirable feature for implant and scaffold design. In this context, the ultrasoft surface of pNE coatings supports stronger and more uniform adsorption of ECM proteins, which play a central role in guiding stem cell attachment and spreading.<sup>70</sup> This is particularly important for pluripotent stem cells, which rely heavily on well-organized ECM cues. This behavior was confirmed by showing that pNE coatings significantly enhanced the adhesion and proliferation of human induced pluripotent stem cell-derived mesenchymal stem cells (hiPS-MSCs) compared to pDA.<sup>71</sup> Moreover, pNE combination of smooth morphology and hydrophilic character also promotes favorable cell–material interactions, resulting in improved adhesion and viability across a range of cell types, including human neural stem cells,<sup>72</sup> NIH-3T3 fibroblasts,<sup>73</sup> hepatocytes,<sup>74</sup> and human pluripotent stem cell.<sup>70</sup> Consistent with this, pLD's increased surface wettability translated into markedly improved cell adhesion and proliferation, particularly for sensitive primary human proximal tubule cells, which typically require optimized, cytocompatible interfaces for successful culture.<sup>64</sup> This is attributed to the fact that pLD-modified surfaces promote greater adsorption of collagen IV and serum proteins like BSA and fibronectin, compared to controls.<sup>46,64</sup> Lastly, pEP preliminary studies have confirmed its biocompatibility, with high cellular viability observed even at elevated concentrations, indicating good compatibility with biological environments.<sup>75,76</sup> However, studies on pEP as a coating are limited and remain at the preliminary stage.

Collectively, these *in vitro* findings emphasize the versatility of polycatecholamine coatings in improving cellular adhesion and viability across diverse cell types. Building on this, an important direction of application lies in bone regeneration, where surface modifications directly influence osteointegration and the immune microenvironment at the implant interface. For example, titanium and its alloys (*e.g.*, Ti<sub>6</sub>Al<sub>4</sub>V), the gold standard in medicine, exhibit a limited inherent bioactivity both *in vitro* and *in vivo*, which significantly improves when coated with polycatecholamines. For example, pDA film on nanoporous titanium enhanced human MG63 osteoblastic cell proliferation by influencing cell adhesion, morphology and RhoA expression, ultimately promoting cell spreading and viability.<sup>77</sup> Notably, even the application of pLD in bone interfaces has been well documented.<sup>46,78</sup> Liu *et al.* showed that zirconia implants coated with pLD promoted osteoblast-like cells MG63 adhesion, cytoskeletal organization, cell proliferation, and ALP expression, outperforming uncoated surfaces.<sup>46</sup> These effects were further amplified when the pLD coating was formed at 37 °C rather than room temperature, a condition that improved protein adsorption, surface wettability, and overall cellular response by accelerating L-DOPA polymerization and enhancing the functionalization of the zirconia surface.<sup>46</sup> pNE has also been explored for bone-related systems by evaluating its effect on MG-63 osteoblast-like cells.<sup>79</sup> The authors observed that after 24 hours, pNE-coated scaffolds exhibited a

greater number of adhering cells compared to pDA-coated surfaces, suggesting more favorable surface properties for initial adhesion. While the overall viability of cells remained comparable across pNE, pDA, and plasma treatments, this enhanced attachment points to subtle advantages in the interfacial compatibility of pNE.<sup>79</sup> These observations in human MG63 cells are consistent with results in other osteogenic models. In mouse MC3T3-E1 pre-osteoblasts, pDA coatings promoted adhesion and early osteogenesis on 3D-printed porous Ti<sub>6</sub>Al<sub>4</sub>V scaffolds.<sup>80</sup> Similarly, pNE coatings have been shown to promote osteoinduction in MC3T3-E1, significantly increased ALP activity compared to pristine polyetheretherketone (PEEK), and support early osteogenic differentiation.<sup>81</sup>

Further research has also highlighted how pDA coatings improve osteogenesis, cell adhesion, and proliferation.<sup>82,83</sup> These beneficial effects are mediated by the pDA redox process, which involves a dynamic switching reaction between the oxidized and reduced forms of pDA. The redox-switchable surface potential of pDA, derived from its phenolic and quinone groups, regulates osteoblast functions relevant to osteogenesis.<sup>82</sup> Specifically, the quinone-rich state enhances osteoblast spreading and proliferation, whereas the phenolic-rich state promotes osteogenic differentiation.<sup>82</sup> Additionally, the primary degradation product of pDA, dopamine, has been shown to inhibit osteoclast differentiation at micromolar or even lower concentrations *via* D2-like receptor signaling, thereby reducing particle-induced osteolysis.<sup>84</sup> While these redox-mediated, structure–function relationships are increasingly well characterized for pDA, analogous mechanistic studies are still largely lacking for pNE and pLD. Given their structural similarity to polydopamine, it is plausible that analogous redox-dependent mechanisms operate in these polymers, though this remains to be experimentally confirmed. It would also be valuable to examine the degradation products of pNE and pLD to determine whether they elicit comparable biological effects to those reported for pDA. For pDA, the *in vitro* results were also replicated *in vivo* where pDA-modified polyetheretherketone implants showed enhanced bone formation and osseointegration in a rat femoral condyle model after four weeks, with greater bone implant contact than bare PEEK.<sup>61</sup> Given that both pNE and pLD exhibit comparable or even superior cellular responses relative to pDA, future studies should extend these findings to *in vivo* systems to establish their translational potential.

In addition to their direct effects on bone cells, both pNE and pDA also exhibit immunomodulatory activity that contributes to tissue regeneration. The inflammatory phase following implantation plays a key role in determining bone healing outcomes, as macrophage polarization toward an anti-inflammatory, pro-healing M2 phenotype promotes osteogenic signaling.<sup>81,85</sup> pDA coatings facilitate this M2 polymerization by suppressing pro-inflammatory cytokines (TNF- $\alpha$  and IL-6) and increasing IL-10 secretion.<sup>85</sup> In parallel, pNE demonstrates comparable immunomodulatory behavior: it reduces M1-associated cytokines (TNF- $\alpha$ , IL-1 $\alpha$ ) and upregulates IL-10, even in the absence of calcium ions, creating a microenvironment



favorable for osteogenesis.<sup>81</sup> When RAW264.7 macrophages were stimulated with lipopolysaccharide, pNE-coated PEEK surfaces significantly decreased the production of TNF- $\alpha$  and IL-1 $\alpha$ , while increasing levels of IL-10 compared to unmodified PEEK.<sup>81</sup> In an interesting comparative study, pNE surpassed pDA, exhibiting significantly lower TNF- $\alpha$ , IL-6, and IL-1 $\beta$  and higher TGF- $\beta$ 1 and IL-10, indicating superior histocompatibility.<sup>63</sup> While among the three polycatecholamines (pDA, pLD and pNE), pLD was the most pro-inflammatory.<sup>63</sup> These findings confirmed that surface functional groups regulate macrophage behavior: carboxylated pLD tends to enhance pro-inflammatory signaling, whereas the hydroxyl-rich pNE surface favors anti-inflammatory activity.<sup>63</sup>

Outside its intrinsic bioactivity, the application of pDA also facilitates the immobilization of proteins and growth factors on the surface of implantable biomaterials and scaffolds, further enhancing its osteogenic potential.<sup>40,86,87</sup> Importantly, the biological activity of these biomolecules has been preserved whether they are immobilized on a pre-formed pDA layer or introduced during the self-polymerization process.<sup>88</sup> However, similarly to pDA, alternative polycatecholamines contain reactive quinone groups that enable covalent immobilization of amine- or thiol-containing biomolecules without requiring additional coupling agents. Their smoother and more hydrophilic surface is poised to improve the accessibility and functional stability of immobilized molecules. For example, on titanate nanotubes, pNE coatings immobilized less catalase than pDA yet delivered higher relative enzyme activity, attributed to reduced steric hindrance on the smoother, more hydrophilic pNE surface.<sup>89</sup> Similarly, dopamine-treated titanium surfaces immobilized more bone morphogenetic protein-2 than L-DOPA-treated ones, yet osteogenic expression was comparable, suggesting that accessibility can compensate for lower loading.<sup>90</sup> Collectively, these data indicate that while pDA may maximize loading, pNE and pLD can preserve or enhance functional activity *via* improved accessibility. However, head-to-head quantitative comparisons remain limited and warrant systematic studies.

Beyond bone applications, polycatecholamines have also been used to support the *in vitro* adhesion and differentiation of neural cells.<sup>65,91–95</sup> Notably, PC12 neuron-like cells were employed across studies with all three polycatecholamines.<sup>93–95</sup> When stimulated with nerve growth factor (NGF), pDA-modified surfaces promoted stronger PC12 adhesion and neuronal differentiation than other surface treatments such as poly-L-lysine or plasma activation.<sup>94</sup> Comparable effects were observed for pNE coatings, which enabled collagen immobilization and localized NGF enrichment, leading to significantly improved neurite number and length compared with collagen-only controls.<sup>93</sup> However, in the absence of NGF stimulation, pNE alone did not induce neurite outgrowth, confirming its dependence on neurotrophic signaling.<sup>93</sup> pLD coatings, by contrast, enhanced cytoskeleton organization even without NGF and, under NGF stimulation, promoted full neuronal differentiation through activation of the NGF/Trk-mediated Rho GTPase pathway.<sup>95</sup> These *in vitro* findings were mirrored

*in vivo*.<sup>66,92,96</sup> Novel decellularized extracellular matrices (dECM) and pDA-coated 3D printed polycaprolactone (PCL)-based conduits displayed neuronal differentiation of Schwann cells, ultimately eliciting nerve regeneration capabilities.<sup>92</sup> Likewise, pDL-modified micropatterned poly(lactic-co-glycolic acid) (PLGA) conduits demonstrated extensive S100-positive Schwann-cell migration.<sup>66</sup> Interestingly, the extent of S100-positive cell coverage in this group closely matched levels observed in autograft controls. The pLD-modified conduits also promoted superior functional recovery, with enhancements observed in electrophysiological performance, sciatic function index, muscle fiber diameter, and axonal innervation density, confirming the therapeutic potential of pLD-based neural conduits.<sup>66</sup> Other than peripheral repair, pLD coatings also showed selective activation of astrocytes proliferation in central nervous system models *via* the L-DOPA-sensitive GPR143 receptor, while maintaining normal neuronal function. A benefit not observed with soluble L-DOPA, which was cytotoxic under equivalent conditions.<sup>65</sup> These results highlight how subtle differences in catecholamine structure can direct distinct neural functions, from adhesion-mediated differentiation to receptor-mediated glial activation, underscoring their versatility for neuroregenerative design.

Building on its success in nerve regeneration, pDA has also been applied to muscle tissue engineering, where its ability to preserve the electrical conductivity of composite materials broadens its functional scope. Although pDA itself is not intrinsically conductive, it facilitates charge transfer when integrated with conjugated polymers such as polypyrrole (PPY).<sup>97</sup> pDA's catechol-rich interphase improves interfacial coupling and charge transport within the conjugated  $\pi$ -network.<sup>97,98</sup> The resulting electroconductive hydrogel also exhibited thermoresponsive gelling properties, together with enhanced cell adhesion and antioxidant capabilities.<sup>97</sup> pDA's antioxidant capacity arises from its catechol/quinone redox cycling, which effectively scavenges a range of reactive oxygen species (ROS) and free radicals, particularly hydroxyl radicals, thereby lowering oxidative stress levels.<sup>99,100</sup> Apart from its role in conductive composites, pDA itself has demonstrated intrinsic bioactivity in promoting myogenic differentiation. On aligned PCL nanofibers, pDA coatings significantly increased the expression of myogenic proteins (myosin heavy chain and myogenin) in C2C12 cells compared to uncoated counterparts.<sup>101</sup> In a similar context, pNE-coated PCL electrospun scaffolds were evaluated for skeletal muscle repair, demonstrating enhanced myocyte adhesion and proliferation, along with *in vivo* regeneration that produced tissue structure and tensile strength approaching those of native muscle.<sup>102</sup> Mechanistically, pNE coatings were found to downregulate myostatin while activating the IGF-1/PI3K/AKT signaling cascade, which is central to muscle growth and hypertrophy, suggesting that pNE can play an active role in modulating regenerative pathways.<sup>102</sup>

Polycatecholamines have also been applied to improve the performance of vascular prostheses, by enhancing blood compatibility and supporting endothelialization.<sup>63</sup> Across multiple



studies, pLD coatings have been shown to reduce hemolysis, coagulation, and cytotoxicity, while significantly improving the viability and adhesion of human umbilical vein endothelial (HUVEC) cells.<sup>47,103,104</sup> In a head-to-head comparisons, as shown in Fig. 3C, HUVEC adhesion and metabolic activity on pLD were higher than on pDA and comparable to pNE.<sup>63</sup> Both pLD and pNE also showed superior hemocompatibility relative to pDA, with pNE performing best overall.<sup>63</sup> This lower hemocompatibility of pDA is attributed to its tendency to induce greater platelet adhesion and more pronounced activation, making additional anticoagulant modification advisable for blood-contacting devices coated with pDA.<sup>63</sup> Mechanistically, a positive surface charge was reported to enhance platelet activation through factor VII activating protease.<sup>105</sup> Consistent with this, pDA, with the greatest density of protonatable amines among the three, elicited stronger platelet responses than pLD or pNE.<sup>63</sup>

Although pLD and pNE often match or surpass pDA in specific properties, many applications have been explored primarily with pDA, leaving a noticeable gap for the other polycatecholamines. In fact, in addition to applications in bone, neural, muscle and vascular tissue engineering, pDA functionalization is also used in cartilage,<sup>106–108</sup> tendon repair<sup>109</sup> and skin regeneration.<sup>110</sup> In skin, pDA intrinsic antioxidative properties play a key role and can be further enhanced by combining it with other antioxidants.<sup>111</sup> This ROS-scavenging capacity accelerates the wound healing process, particularly following the inflammatory phase. Zhang *et al.* demonstrated the efficacy of pDA-coated scaffold outperforming both uncoated controls and commercial dressings (*e.g.*, 3M's Tegaderm™) in promoting rat skin wound healing.<sup>110</sup> Also for tendons, silk fibroin nanofibers modified with pDA were shown to alleviate oxidative stress and inflammation during early repair, while simultaneously inducing remodeling and regeneration.<sup>109</sup>

**Outlook.** Among the biomedical applications of polycatecholamines, surface modification remains the most widely used, with pDA serving as the benchmark material due to its broad applicability, redox reactivity, and ease of deposition. However, recent comparative studies have demonstrated that alternative polycatecholamines, particularly pLD and pNE, exhibit distinct surface properties that may offer advantages for specific biomedical applications.<sup>28,63</sup>

From a material perspective, pLD has shown greater physicochemical stability, particularly under acidic and basic conditions where pDA tends to degrade.<sup>22</sup> Meanwhile, pNE has demonstrated enhanced hydrophilicity, smoother surface morphology and better macrophages polarization compared to pDA.<sup>38,63</sup> Moreover, although antioxidant and conductive behaviors have so far been attributed primarily to pDA, they arise from the catechol/quinone redox system common to all polycatecholamines. The antioxidant properties of pNE have been experimentally verified but only at the material level. pNE coatings on polypropylene exhibited an antioxidant capacity equivalent to 11.72 mmol per L FeSO<sub>4</sub> per cm<sup>2</sup>, consistent with redox activity surface catechol groups.<sup>112</sup> However, direct cellular evidence (such as reduced intracellular ROS) has not been

reported for pNE. In contrast, pLD NPs have recently shown quantitative antioxidant activity both in chemical and biological systems.<sup>113</sup> ABS and DPPH assay revealed substantially lower EC<sub>50</sub> values than pDA, and in HUVEC models, pLD nanoparticles provided significant ROS suppression, confirming true biological antioxidant behaviour.<sup>113</sup> It is thus plausible that both pNE and pLD share comparable redox responsiveness, with their structural differences potentially amplifying these effects. The extra hydroxyl group in pNE and the carboxyl group in pLD could modulate electron delocalization and stabilize intermediate oxidation states, enhancing radical scavenging and charge-transfer efficiency. Consequently, these polymers may extend the functional reach of surface coatings beyond simple biocompatibility toward redox-active and electroresponsive interfaces. These properties, combined with the overall cytocompatibility and functionalizability of both polymers, suggest that pLD and pNE coatings may be applied to those biomedical contexts where pDA has already shown promise (such as cartilage, tendon, and skin) but where improved surface smoothness, ligand accessibility, and/or pH stability are required for added benefits.

In this context, pNE's combined ROS-scavenging potential and demonstrated immunomodulatory activity position it as a strong candidate for coatings that modulate both oxidative and inflammatory stresses, aspects that are particularly relevant for skin and tendon regeneration, where pDA has already achieved *in vivo* success. By concurrently mitigating ROS accumulation and directing macrophages toward the M2 phenotype, pNE could further stabilize wound interfaces and accelerate matrix remodeling beyond what is observed with pDA.

pLD's chemical robustness and smooth conformality make it a compelling alternative to pDA for osteochondral interfaces. Bone-side acidity can destabilize pDA, whereas pLD remains stable across a wide pH range and preserves interfacial chemistry.<sup>22</sup> On the cartilage side, pLD's uniform, hydrophilic surface supports predictable protein conditioning (collagen, fibronectin) and improves adhesion/proliferation of sensitive primary cells,<sup>46,64</sup> minimizing roughness-driven nonspecific adsorption. Collectively, pLD could promote matrix continuity and graded adhesion and enable spatially controlled immobilization of cues.

Conversely, pEP remains significantly underexplored for surface modifications. Films are less cohesive and buffer-sensitive,<sup>11,25</sup> but its cytocompatibility, even at high concentrations,<sup>75,76</sup> highlight its potential for surface modification strategies that prioritize transient adhesion.

### Bioadhesive technologies

Traditional methods of wound closure, such as sutures, staples and clips, may lead to secondary tissue damage and microbial infection. With the development of modern medicine, clinical requirements for wound treatment have become increasingly demanding. Efforts are made not only to alleviate pain and shorten wound healing time, but also to restore tissue function and appearance.<sup>114</sup> Bioadhesives, based on natural (*e.g.*, polysaccharides, proteins) or synthetic polymers



(e.g., cyanoacrylate, polyethylene glycol, polyurethane), offer significant potential.<sup>115</sup> These materials form a protective layer that maintains continuous adhesion between injured tissues, ensuring a more effective wound closure while creating a beneficial microenvironment for healing.<sup>116</sup> In addition to a low risk of infection and rapid healing, these bioadhesives can provide a physiological environment similar to the natural extracellular matrix for proliferation and differentiation, which is superior to traditional wound closure methods.<sup>114</sup> However, a significant challenge lies in balancing the biocompatibility and adhesion strength of these materials. Natural polymers, while generally more cytocompatible compared to synthetic ones, often lack adequate adhesion strength, especially in a wet environment such that of tissues and organs.<sup>116</sup> Polysaccharide-based adhesives, for instance, have excellent tissue-mimicking features but insufficient adhesiveness.<sup>117</sup> On the other hand, synthetic adhesives, such as cyanoacrylates, offer strong adhesion but are less biocompatible.<sup>1</sup>

To address these limitations, pDA has emerged as a highly effective component in the development of bioadhesives due to its unique adhesive properties, especially under wet conditions, and its biocompatibility. The catechol groups in pDA

supports various chemical interactions and crosslinks, especially with nucleophilic groups on tissue surfaces (Fig. 4A), significantly enhancing adhesion strength.<sup>117,120</sup> Studies have demonstrated that incorporating pDA into various materials improves their adhesive properties, making them suitable for applications in wound closure and tissue repair. For example, pDA-incorporated composites have shown enhanced adhesion on both dry and wet surfaces, with adhesive strengths typically ranging from 20 to 50 kPa as measured by lap-shear adhesion tests.<sup>118,121–124</sup> As shown in Fig. 4B, these values are comparable to those of commercial bioadhesives such as Eviceal™ (26 ± 4 kPa) and Coseal™ (19 ± 7 kPa).<sup>118</sup> Notably, when pDA is synthesized as nanoparticles (NPs), adhesive properties depend on their size and concentration.<sup>125</sup> Specifically, optimal adhesion was observed with smaller nanoparticles (200 nm in diameter).<sup>125</sup> Increasing the NPs concentration further improved adhesion, with a concentration of 20% w/v reaching an adhesive strength of 52.56 ± 3.04 kPa, an improvement of approximately 163%.<sup>125</sup>

The promotion of wound regeneration by pDA-functionalized hydrogels has been observed across multiple studies.<sup>126,127</sup> These composite materials outperformed the

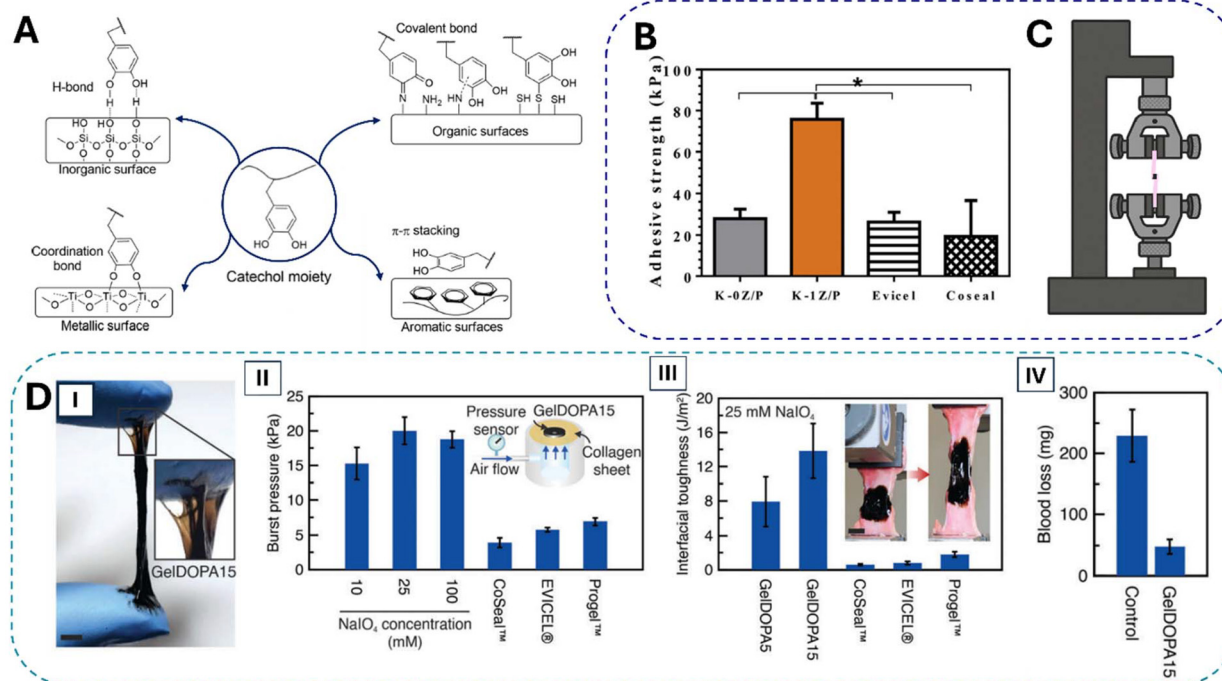


**Fig. 4** (A) Common interaction mechanisms between catechol and various surfaces. Adapted with permission from ref. 59. Copyright 2019 American Chemical Society. (B) Quantified adhesive strength measured by lap shear testing (cross head rate 1 mm min<sup>-1</sup>) for the K-1Z/P hydrogel (composed of kappa-carrageenan and polydopamine-modified ZnO nanoparticles) compared to the control K-0Z/P hydrogel (without ZnO) and two commercial bioadhesives (Eviceal™ and Coseal™). Reprinted from ref. 118, with permission from Elsevier. Copyright 2020 Elsevier. (C) Schematic illustration of the lap shear test setup, in which the hydrogel sample is placed between two overlapping substrates and subjected to tensile force until failure. (D) (I) Visual demonstration of GelDOPA15's strong tackiness, adhering to surgical gloves. Scale bar = 5 mm. (II) *In vitro* burst pressure test evaluating the adhesive strength of GelDOPA on collagen sheet substrates (III) Wound closure test conducted on porcine lung tissue at a cross-head rate of 25 mm min<sup>-1</sup> (scale bar = 5 mm). (IV) Quantitative results from an *in vivo* mouse liver bleeding model demonstrating the ability of GelDOPA bioadhesives to reduce bleeding, attributed to their rapid thermal gelation and strong tissue adhesion. Adapted with permission from ref. 119. Copyright 2023 Wiley.



commercial 3T Tegaderm™ in promoting wound healing and collagen fiber organization in the dermis, highlighting enhanced dermal remodeling and maturation.<sup>127</sup> Moreover, in a full-thickness wound on the dorsal side of rats, histological analysis revealed that pDA–HA group had better-organized collagen fibers and a reduced  $\alpha$ -SMA positive area compared to the HA-only group, indicating that pDA reduced scar formation.<sup>126</sup> Notably, pDA's regenerative capacity extends to particularly challenging sites such as the oral mucosa<sup>124</sup> and enterocutaneous fistulas<sup>122</sup> where conventional adhesives often fail.

Among polycatecholamines, pLD remains the only one reported in bioadhesive design, while pNE and pEP have not yet been explored in this context. pLD's intrinsic low hemolysis, high drug-retention capacity, and promotion of cell proliferation make it a promising functional additive for the development of bioadhesive materials used in applications such as wound dressings<sup>128,129</sup> and surgical glues.<sup>119,130</sup> As shown in Fig. 4D, the incorporation of poly-L-DOPA can significantly enhance the adhesive properties of both synthetic systems (such as cyanoacrylate)<sup>130</sup> and natural matrices (such as gelatin).<sup>119</sup> Montazerian *et al.* explored this in depth, showing that pre-polymerized pLD conjugated to gelatin (GelDOPA) increased catechol density and enabled rapid gelation ( $\sim 10$  s), strong burst adhesion, and *ex vivo* sealing of porcine lungs and bladders.<sup>119</sup> Specifically, interfacial toughness, measured *via* wound-closure test on porcine lung, was  $\sim 13 \text{ J m}^{-2}$  for GELDOPA15, about 10–15 times higher than commercial sealants (Evicel®, Progel™, Coseal™), as shown in Fig. 4D. Likewise, *in vitro* burst-pressure testes showed  $\sim 3$ - to 5-fold higher adhesion compared to commercial bioadhesives and *ex vivo* porcine lung burst pressure was  $\sim 2$ - to 4-fold higher and also exceeded gelatin methacrylate (GelMA). These improvements are largely attributed to the carboxylic acid groups in L-DOPA, which provide additional hydrogen bonding and electrostatic interaction sites, strengthening both cohesion and surface adhesion.<sup>119</sup> In addition to enhancing tissue adhesion strength, the presence of pLD consistently improves cell viability and overall biocompatibility, even outperforming commercial surgical sealants such as Evicel™ while showing lower cytotoxicity than fibrin glue.<sup>119,129,130</sup>

The improved adhesion also contributes to stabilizing the wound site and forms a physical barrier, promoting clot formation. Additionally, the presence of catechol groups in pDA further supports hemostasis by triggering the coagulation cascade.<sup>131</sup> Li *et al.* demonstrated that pDA-incorporated cryogels significantly reduced blood loss *in vivo* in a rabbit liver volume defect model, with an  $\sim 80\%$  reduction compared to the control.<sup>123</sup> Moreover, pDA exhibits effective hemostatic properties both *in vitro* and *in vivo*, even in NPs form.<sup>124</sup> Similarly, GelDOPA effectively adhered to actively bleeding tissue and significantly reduced blood loss (up to  $\sim 75\%$ ) in a mouse liver injury model, highlighting its strong hemostatic potential (Fig. 4D).<sup>119</sup>

In addition to their hemostatic effects, catechol-based bioadhesives also contribute to infection control. For instance, polydopamine-coated zinc oxide NPs not only displayed hemo-

static activity but also conferred antibacterial properties; an essential dual function for promoting infection-free wound healing.<sup>124</sup> In this context, the antibacterial effects of pDA arise from multiple mechanisms. Specifically, (i) metal ions essential for bacterial metabolism are chelated by catechol groups in pDA,<sup>133</sup> and (ii) its protonated amine groups interact electrostatically with negatively charged bacterial membranes, leading to cell lysis.<sup>133</sup> Lastly, (iii) pDA's redox-active catechol/quinone network can transfer electrons to  $\text{O}_2$  to generate ROS, contributing to membrane-damaging antibacterial action.<sup>134</sup> Alongside pDA, with the exception of pLD (Fig. 5A),<sup>119</sup> other polycatecholamines also show intrinsic antibacterial properties. Specifically, pNE-grafted surfaces reduced bacterial colonization by disrupting membrane integrity and inhibiting adhesion.<sup>112</sup> This effect is likely mediated by electrostatic interactions between protonated amino groups on the pNE surface and negatively charged bacterial membranes,<sup>112</sup> similar to one of the known antibacterial mechanisms of pDA. Moreover, pEP-containing coatings demonstrated strong, broad-spectrum bactericidal activity without any additional antimicrobials.<sup>35</sup> Interestingly, pEP showed nearly complete eradication ( $>99\%$  lethality) of both Gram-positive and Gram-negative strains, even against methicillin-resistant *Staphylococcus Aureus* (Fig. 5B).<sup>35</sup> The effect was accompanied by pronounced bacterial membrane deformation, consistent with a membrane-disruptive mechanism.<sup>35</sup>

In contrast to the pronounced bactericidal effect reported for pEP, the intrinsic antibacterial activity of pDA, pLD, and pNE tends to be more modest, and it is often enhanced with additional agents or through external stimuli. For example, their photothermal properties allow for the conversion of light energy into heat upon near infrared (NIR) irradiation, effectively damaging bacterial membranes.<sup>135</sup> This photothermal behaviour is well characterized for polydopamine and it is attributed to its conjugated structures and electron donor-acceptor interactions, especially between 5,6-dihydroxyindole and indole-5,6-quinone moieties.<sup>133</sup> Consistent with this, both pNE and pLD reached bactericidal temperature under NIR, as shown in Fig. 5B, closely matching pDA (pNE  $\sim 63$  °C; pLD  $\sim 65$  °C; pDA  $\sim 65$  °C).<sup>119,132</sup> Importantly, in a comparative study, both pNE and pDA coatings exhibited excellent thermal stability across multiple irradiation cycles, confirming their reliability for repeated use. This photothermal strategy was effective against both *S. aureus* and *E. coli*, with pNE showing similar efficacy to pDA against *S. aureus* and outperforming it against *E. coli* (Fig. 5C).<sup>132</sup> Moreover, the abundance of catechol and amine structures in pDA facilitates the loading of additional antibacterial materials such as metals for synergistic effects.<sup>86</sup> This metal-driven improvement combined with NIR activation was observed by Yang *et al.*, who used copper NPs in combination with pDA. Their study confirmed that pDA significantly enhanced the antibacterial properties of Cu NPs.<sup>136</sup> A similar concept was applied using pDA as a coating in a 3D printed hydrogel composed of dopamine-grafted on GelMA and reduced graphene oxide.<sup>137</sup> The hydrogel showed significant antibacterial activity even without NIR light.



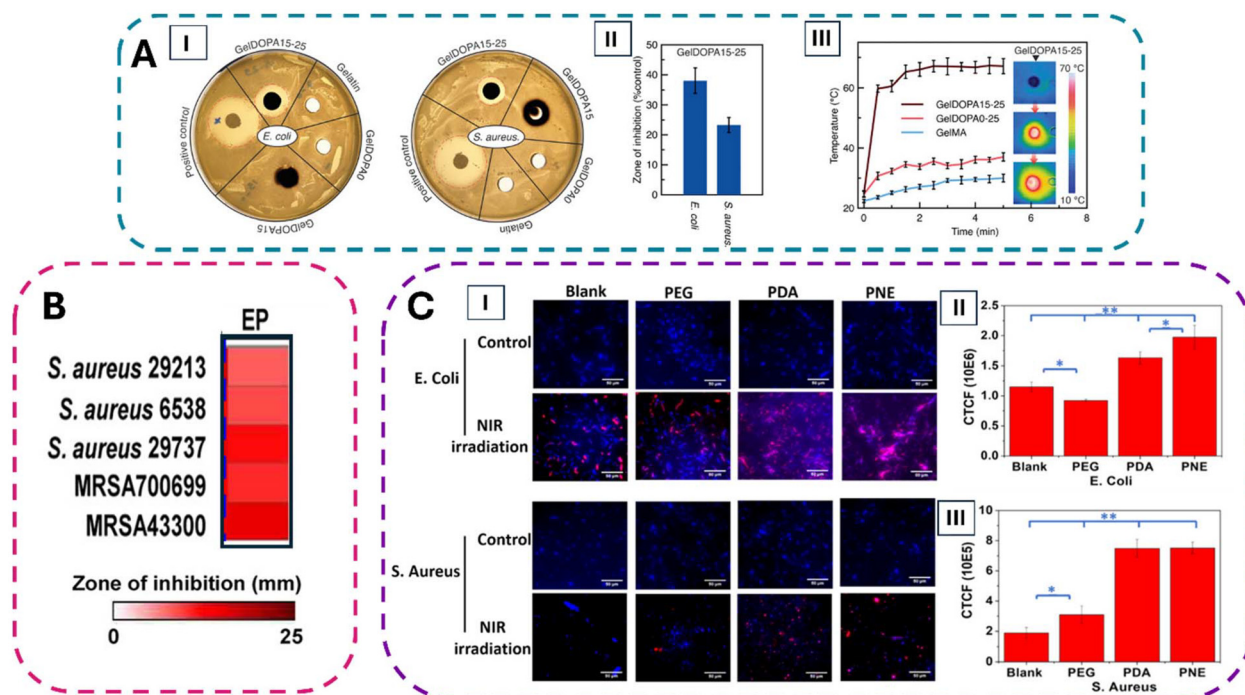


**Fig. 5** (A) (I) Antibacterial zones of inhibition for uncrosslinked GelDOPAx samples ( $x = \text{mg of NaIO}_4$  per 10 mL used to polymerize L-DOPA during GelDOPA synthesis) and crosslinked GelDOPAx- $y$  samples ( $y = \text{NaIO}_4$  concentration in mM used to crosslink GelDOPAx). For the positive control, 8 mm filter paper disks were impregnated with silver sulfadiazine (15  $\mu\text{g}$  per disk) and placed on the plates. (II) Relative inhibition-zone area of GelDOPA15-25 compared to the positive control against *E. coli* and *S. aureus*. (III) Temperature response of GelDOPA hydrogels in wet media under NIR irradiation (808 nm, 6 W for 10 min); insets show thermal images of GelDOPA15-25 during NIR exposure. Adapted with permission from ref. 119. Copyright 2023 Wiley. (B) Heat map showing zones of inhibition for polyepinephrine (EP) films against five Gram-positive *S. aureus* strains. The color scale indicates inhibition-zone diameter (mm). Adapted with permission from ref. 35. Copyright 2016 American Chemical Society. (C) (I) Fluorescence images of *E. coli* and *S. aureus* adhered to four types of coverslips (blank, PEG-coated, pDA-coated, and pNE-coated) after 24 h incubation, without (Control) and with NIR irradiation (850 nm, 1 W  $\text{cm}^{-2}$  for 10 min). Blue signal corresponds to total bacteria (live + dead), while red signal represents propidium iodide (PI)-stained dead bacteria. Scale bar = 50  $\mu\text{m}$ . (II, III) Quantification of PI fluorescence for *E. coli* (II) and *S. aureus* (III) expressed as corrected total cell fluorescence (CTCF) measured in ImageJ. \* $P < 0.05$  and \*\* $P < 0.005$ . Adapted with permission from ref. 132. Copyright 2020 American Chemical Society.

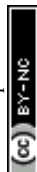
However, NIR irradiation further improved this activity, achieving nearly complete bacterial eradication. *In vivo* testing of the hydrogel on a full-thickness infected wound in rats further confirmed both antibacterial efficacy and wound healing properties.<sup>137</sup> Likewise, pLD has proven effective for antibiotic loading. In particular, pLD-functionalized  $\beta$ -glucan hydrogels showed to significantly improve gentamicin retention, suggesting that these materials could be ideal for treating hard-to-heal bleeding wounds at risk of infection.<sup>128</sup> The pLD-modified hydrogel immobilized greater gentamicin amounts (3970–5479  $\mu\text{g g}^{-1}$ ) and extended antibacterial protection to 44 days, compared to 3164–3773  $\mu\text{g g}^{-1}$  and 28 days for pDA-modified controls, indicating superior antibiotic binding and prolonged efficacy.<sup>128</sup>

**Outlook.** pDA remains the most extensively studied polycatecholamine for bioadhesive applications, owing to its strong cohesive properties and exceptional wet adhesion. Its ability to form DHI units during oxidative polymerization enables  $\pi$ - $\pi$  stacking and cation- $\pi$  interactions, contributing to its high film-film adhesion and robustness, as demonstrated through surface force apparatus measurements.<sup>138</sup> This robust wet

adhesion is clinically critical, especially in internal surgical settings, such as bleeding control and tissue sealing. pDA-based adhesives have been successfully applied in internal biomedical settings, including uterine membranes, skin wounds, enterocutaneous fistulas, and hemostatic agents, where they exhibit adhesion strengths comparable to or exceeding FDA-approved products such as Coseal<sup>TM</sup> and Eviceal<sup>TM</sup>.<sup>118,122,123,126,139</sup>

In contrast, pEP is currently not considered a suitable candidate for bioadhesive applications. The lack of DHI units in pEP, which normally enable extensive  $\pi$ - $\pi$  stacking and strong cohesive forces, results in films that are structurally less robust and more sensitive to degradation. Nevertheless, given its potent, broad-spectrum antibacterial activity even against resistant strains,<sup>35</sup> pEP could find niche applications in high risk contaminated wounds or short-term dressings where rapid bacterial eradications outweighs the need for long-term mechanical stability. For example, in acute burn care, a short-lived antibacterial dressing can rapidly reduce bioburden to create a cleaner wound bed for subsequent tissue repair.

The other two polycatecholamines examined in this work, namely pLD and pNE, are promising candidates. Building on



the success of pDA, pLD has emerged as a potent alternative. Formulations such as GelDOPA have demonstrated excellent tissue sealant behavior, even outperforming commercial products like Coseal™, Evice™, and Progel™.<sup>119</sup> pLD's carboxylate group significantly enhances its biofunctionalization capacity, allowing for stronger interactions with biomolecules and tissue interfaces.<sup>119,128</sup> That said, the volume of published research on pLD remains significantly smaller than that for pDA, and its application landscape is still in development. Expanding its use across tissues where pDA has already proven effective, such as mucosal interfaces or enterocutaneous applications, represents a promising direction for future exploration.

Conversely, pNE remains notably underexplored as a bioadhesive, despite possessing surface and biological properties that suggest considerable promise. Its additional  $\beta$ -hydroxyl group may enhance hydrogen bonding with tissue surfaces, and its coatings have been shown to be ultrasmooth, hydrophilic, and bioactive.<sup>38,81</sup> Moreover, pNE exhibits photothermal antibacterial effects comparable to pDA when irradiated with NIR light, supporting its potential in infected or open wound environments.<sup>132</sup> Beyond surface adhesion, pNE exerts direct bioactive effects on muscle tissue, having been shown to downregulate myostatin and activate the IGF-1/PI3K/AKT signaling pathway, a critical axis for muscle regeneration and hypertrophy.<sup>102</sup> This suggests pNE could be strategically developed as a muscle-specific or regenerative bioadhesive, particularly for internal applications where few FDA-approved adhesives currently exist.

### Biosensors

Biosensors are analytical devices that integrate biological recognition elements (such as enzymes, nucleic acids, antibodies, and cells) with transducers, enabling real-time, specific, and sensitive detection of target analytes. When an analyte interacts with a biological recognition element, this interaction induces a measurable physical or chemical change that is detected by the transducer and converted into a quantifiable readout. These devices are typically classified based on their transduction mechanisms, such as optical, electrochemical, piezoelectric, and thermal biosensors. Among these, optical and electrochemical biosensors are currently the most extensively utilized in biomedical applications.<sup>140</sup>

The most important requirements of biosensors are sensitivity and selectivity. Polycatecholamines directly address the former, as their quinone and hydroquinone functional groups facilitate effective biomolecule–matrix electron transfer, ultimately amplifying signal transduction.<sup>141</sup> Additionally, the abundance of these functional groups enables covalent immobilization of recognition elements (*e.g.* DNA, enzymes, or antibodies) through Schiff-base or Michael addition reactions. Together these features provide a stable and efficient interface that supports both sensitivity by improving signal transduction and selectivity by ensuring specific and oriented binding of the target molecules.<sup>142</sup> Selectivity can be further improved by employing molecularly imprinted (MIP) polymers, which form highly specific binding cavities tailored to the target analyte.

These significantly reduce interference from structurally similar molecules, thereby enhancing the biosensor's ability to discriminate between analytes.<sup>143</sup>

In this context, polydopamine's ability to adhere to virtually any material without pre-functionalization<sup>5</sup> enables the direct fabrication of surface-imprinted layers on transducers or nanoparticles, improving sensor performance and reusability. pLD has also proven advantageous in MIP for synthetic biorecognition.<sup>144</sup> A potentiometric MIP sensor was developed with electropolymerized pLD as the matrix for levofloxacin imprinting.<sup>144</sup> Also in this case, the catechol and carboxylic acid groups in L-DOPA enable stronger template–matrix interactions, resulting in high imprinting fidelity, enhanced rebinding efficiency, and reduced nonspecific interactions, ultimately improving both selectivity and reproducibility. In addition, pNE has been widely explored as a coating material for MIP strategies. Its more uniform and controlled polymerization compared to pDA results in highly defined molecular cavities, significantly reducing nonspecific binding and enhancing imprinting fidelity and specificity.<sup>145–147</sup> Sestaioni *et al.* demonstrated the substantial economic advantage of pNE-coated sensors, concluding that its rapid and straightforward removal using a mild NaOCl solution within just 60 seconds reduced sensor costs by up to 90%.<sup>146</sup> This rapid removal capability further underscores the practical advantage over the more adherent and difficult-to-remove pDA coatings.<sup>146</sup> Moreover, Torrini *et al.* synthesized spherical pNE (nano-MIPs) for detection of IgG1.<sup>148</sup> The pNE NPs showed significantly improved analytical performance, exhibiting a 4.3-fold higher signal compared to pDA nanoparticles.<sup>148</sup> This superior performance was associated with the distinct polymerization kinetics of pNE, which resulted in smaller, dimensionally stable NPs that retained their uniform size distribution over time.<sup>148</sup> Furthermore, the three-dimensional nanostructure markedly improved binding site accessibility and sensor responsiveness relative to traditional two-dimensional configurations.<sup>148</sup>

Together, these studies underscore how polycatecholamine-based MIP architectures enhance recognition fidelity, binding efficiency and signal strength across multiple sensor formats. These advantages are particularly valuable in electrochemical biosensing, where biological interactions at the electrode interface must be efficiently converted into measurable electrical signals, such as changes in current, conductance, resistance, or potential. Typically, they consist of a three-electrode setup: (i) a reference electrode, (ii) a counter electrode, and (iii) a working electrode onto which the recognition molecule is immobilized. Depending on their specific measurement mode, electrochemical biosensors can be classified into voltammetric, conductometric, potentiometric, or amperometric sensors.<sup>141</sup>

Electrochemical biosensors often operate in complex biological fluids where non-specific adsorption of biomolecules leads to biofouling, significantly impairing sensor performance and long-term stability. Antifouling properties are therefore essential to preserve sensitivity and selectivity over time, enabling the detection of small target molecules while effec-



tively reducing interference from common biological contaminants.<sup>149</sup> In general, polycatecholamines coatings contribute to antifouling behavior due to their hydrophilicity and surface charge characteristics. In fact, they exhibit both protonated amine and deprotonated phenolic or carboxyl groups under physiological pH, imparting zwitterionic-like behavior that reduces non-specific adsorption and promotes biomolecular recognition.<sup>132,142,150</sup> Their antifouling properties can be further enhanced *via* copolymerization with zwitterionic or highly hydrophilic polymers such as poly(sulfobetaine methacrylate)<sup>151</sup> or poly(oligo(ethylene glycol) methacrylate).<sup>152</sup> Notably, as shown in Fig. 6A, pNE has been directly compared to pDA under identical protein-fouling conditions, and it consistently exhibits stronger antifouling activity.<sup>132,147</sup> This behaviour has been attributed to the additional hydroxyl group in the pNE network, which reduces hydrophobic interactions and increases surface hydrophilicity, as well as to its ultra-smooth morphology.<sup>132,147</sup> Together, these features promote the formation of a hydration layer that acts as a physical barrier to protein adsorption.<sup>132</sup> Specifically, in BSA adsorption assays, pNE-coated surfaces showed no detectable proteins after 24 hours, whereas pDA retained residual BSA. Notably, AFM force spectroscopy using a BSA-functionalized tip revealed a substantially lower BSA-surface adhesion energy

for pNE ( $\sim 2 \times 10^{-19}$  J) than for pDA ( $\sim 9 \times 10^{-19}$  J).<sup>132</sup> By contrast, pLD has also shown promising antifouling behaviour in membrane and surface-modification studies,<sup>150,152</sup> owing to its zwitterionic structure and enhanced hydrophilicity. Given the lower contact angles typically reported for pDL coatings<sup>63</sup> compared to pDA, this property would be expected, as it did for pNE, to further contribute to antifouling performance.

While antifouling is crucial to maintain sensor stability in complex media, biosensor performance also depends on how effectively these polycatecholamines films can immobilize bio-recognition elements and support efficient electron transfer. In this context, pDA layers also enable stable antibody immobilization,<sup>151</sup> DNA probes,<sup>154</sup> enzymes<sup>155</sup> which is fundamental for achieving high sensitivity in biomedical applications. However, recent comparative studies have highlighted pLD superior performance in electrochemical systems, especially in applications requiring the immobilization of enzymes.<sup>27,156</sup> The key difference lies in pLD's unique chemical structure: the presence of both catechol and carboxylic acid groups enables richer surface chemistry than pDA.<sup>27,156</sup> Importantly, pLD has proven effective under both electrochemical<sup>27</sup> and enzymatic polymerization conditions,<sup>33,156</sup> consistently outperforming pDA in enzyme entrapment efficiency and biocompatibility. For example, tyrosinase-catalyzed (Tyr) polymerization of

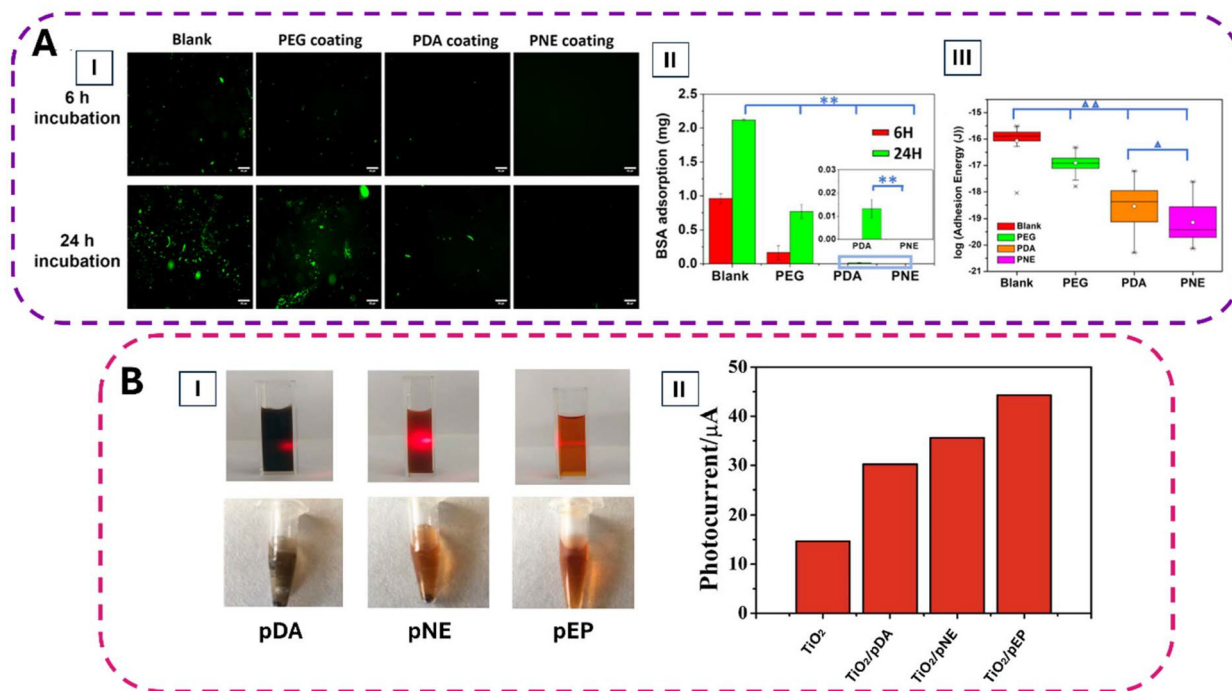


**Fig. 6** (A) (I) Fluorescence images of fluorescein isothiocyanate (FITC)-labeled BSA (FITC-BSA) adsorbed on blank, PEG-, pDA-, and pNE-coated coverslips 6 h and 24 h of incubation (scale bar = 50  $\mu\text{m}$ ). (II) Amount of BSA adsorbed on each surface after 6 h and 24 h, quantified by Bradford assay. (III) Adhesion energy between a BSA-functionalized AFM tip and the different surfaces, calculated from force–distance curves.  $^{\wedge}P < 0.05$  and  $^{**}/^{\Delta\Delta}P < 0.005$ . Adapted with permission from ref. 132. Copyright 2020 American Chemical Society. (B) (I) Photographs of dopamine-, norepinephrine-, and epinephrine-derived melanin-like polymer dispersions (top) under red-laser illumination and after centrifugation at 5000 rpm for 5 min (bottom), showing precipitation for pDA and pNE but a stable dispersion for pEP. (II) Photocurrent response of bare  $\text{TiO}_2$  and  $\text{TiO}_2$  electrodes coated with pDA, pNE, or pEP, showing the enhancement in photocurrent upon polycatecholamine functionalization. Readapted with permission from ref. 153. Copyright 2018 American Chemical Society.



L-DOPA yielded a melanin-like pLD film that served as a superior matrix for enzyme immobilization compared to polydopamine, poly(L-tyrosine), chitosan, and Nafion.<sup>156</sup> In this study, a pLD-Tyr/glassy carbon electrode exhibited a sensitivity of  $4.29 \text{ mA mM}^{-1} \text{ cm}^{-2}$ ; substantially outperforming the pDA-based counterpart ( $1.75 \text{ mA mM}^{-1} \text{ cm}^{-2}$ ).<sup>156</sup> Moreover, the pLD matrix preserved 91.4% of the native enzymatic activity, the highest among all tested matrices.<sup>156</sup> Likewise, the stable polymeric structure of pNE provides abundant redox-active catechol groups and functional moieties for hydrogen bonding. These features together support efficient immobilization of different biomolecular recognition elements and facilitate rapid electron transfer at the electrode interface.<sup>157–161</sup> Analogous to pDA, this enhanced electron transfer arises from the oxidative self-polymerization of norepinephrine, producing quinone moieties that act as redox mediators.<sup>157</sup> In a recent comparative study on rGO electrodes demonstrated that pNE coatings had a higher electroactive surface area (29.4%) than pDA (15.8%) compared to control, higher DNA immobilization, better sensitivity, and enhanced electrochemical responses.<sup>161</sup> This improvement was attributed to pNE's additional hydroxyl group, enabling the formation of twelve resonance structures compared to eight in pDA, thus promoting greater electron delocalization, conductivity, and electrochemical responsiveness.<sup>161</sup> Consistent behaviour was observed in enzymatic biosensors, where pNE-coated magnetite nanoparticles markedly enhanced glucose oxidase immobilization ( $38.4 \text{ mg g}^{-1}$  vs.  $17.3 \text{ mg g}^{-1}$ ) and electrocatalytic activity compared to a pDA-based system.<sup>159</sup> Specifically, the pNE-based sensor exhibited significantly higher sensitivity ( $97.3 \text{ } \mu\text{A mM}^{-1} \text{ cm}^{-2}$  vs.  $1.55 \text{ } \mu\text{A mM}^{-1} \text{ cm}^{-2}$ ) and a lower detection limit ( $6.1 \text{ } \mu\text{M}$  vs.  $115.74 \text{ } \mu\text{M}$ ), while maintaining long-term stability over 20 weeks.<sup>159</sup> Lastly, for pEP a notable study is the biosensor developed by Ma *et al.*, in which they compare pEP, pDA, pNE film deposited onto TiO<sub>2</sub>-modified ITO electrodes with immobilized anti-PSA antibodies on the surface for prostate-specific antigen detection.<sup>153</sup> Under identical alkaline conditions (Tris-HCl buffer, pH 8.5), pEP outperformed pDA and pNE across multiple performance metrics. In terms of dispersion stability, pEP formed a uniform brown solution with no visible aggregation (Fig. 6B), whereas pDA and pNE rapidly precipitated within 30 minutes.<sup>153</sup> Most notably, the photocurrent density of the pEP-coated electrode reached  $1.1 \text{ } \mu\text{A cm}^{-2}$ , compared to  $0.54 \text{ } \mu\text{A cm}^{-2}$  for pDA and  $0.23 \text{ } \mu\text{A cm}^{-2}$  for pNE, under identical illumination conditions.<sup>153</sup> The pEP system also showed strong photoelectrochemical stability, retaining approximately 90% of its photocurrent response after 8 cycles of on-off light exposure.<sup>153</sup> The authors attributed these improvements to pEP's excellent solubility, its ability to form homogeneous, stable coatings, and a film morphology that enhanced light harvesting and charge transport across the electrode interface.<sup>153</sup> This demonstrates the chemical reactivity of pEP films toward biofunctionalization.

Lastly, polycatecholamine films can also act as green reducing and capping agents for *in situ* metal nanoparticle growth, adding another level of signal amplification in biosensing

architectures. By virtue of its catechol and quinone functional groups, pDA chelates metal ions (such as Au<sup>3+</sup> or Ag<sup>+</sup>) and reduces them *in situ* to their metallic form.<sup>162</sup> This redox process is driven by the electron-donating capability of catechol groups, which undergo oxidation to quinone while reducing the metal ions.<sup>8</sup> The resulting metal nanoparticles form stable and uniformly distributed layers directly on pDA-coated surfaces, a mechanism widely exploited in biosensors to enhance conductivity, catalytic activity, and local electromagnetic fields.<sup>162</sup> pLD also offers intrinsic redox activity, which can be harnessed for the *in situ* reduction of metal ions.<sup>27</sup> pLD-coated surfaces were used to reduce HAuCl<sub>4</sub> to gold nanoparticles without the need for external reducing agents.<sup>27</sup> This green, surface-confined synthesis parallels known properties of pDA, but benefits from pLD's carboxylate-rich surface, which can further stabilize metal nanostructures and enable additional surface modifications.<sup>27</sup> Similar to pDA, pNE can effectively chelate metal ions through its catechol moieties, a property leveraged to synthesize metal-doped nanoparticles.<sup>163</sup> Notably, the doping approach using pNE is particularly advantageous due to the presence of an additional  $\beta$ -hydroxyl group compared to dopamine, which provides a higher density of hydroxyl functionalities and thus enhances metal chelation capacity.<sup>163</sup> To date, however, this chelating and reducing capability of pNE remains largely underexplored in electrochemical biosensors. In fact, in the few pNE-based biosensors, the polymer instead functions primarily as an adhesive and functional interlayer that anchors pre-formed metal NPs.<sup>161</sup> A similar picture emerges for pEP, that demonstrated reducing and stabilizing abilities for *in situ* Ag NPs in nanocatalysts applications.<sup>164</sup> Together, these observations suggest that pNE and pEP remain underexploited in biosensor applications, despite their demonstrated ability to chelate and reduce metal ions.

The rich chemical structure of polycatecholamines also plays a central role in optical biosensors. Its functional groups contribute in fact to fluorescence modulation, and metal nanoparticle synthesis, thereby expanding their application in light-based detection systems. Optical biosensors are the most widespread biosensors and rely on changes in light absorption or emission properties triggered by biological interactions. Commonly optical techniques include fluorescence, chemiluminescence, surface plasmon resonance (SPR), surface-enhanced Raman scattering (SERS), and photoacoustic imaging.<sup>165,166</sup>

Fluorescence imaging is among the most extensively utilized and powerful techniques in biosensing, owing to its exceptional sensitivity, selectivity, and spatiotemporal resolution.<sup>166</sup> Intrinsically, pDA exhibits weak auto fluorescent properties with emission typically occurring within the range of 400–550 nm depending on the excitation wavelength and the precursor.<sup>42</sup> This autofluorescence is attributed to its structural similarity with melanin, consisting of numerous aromatic oligomers. Strong  $\pi$ - $\pi$  stacking interactions between these oligomers lead to aggregation-caused quenching.<sup>166</sup> However, synthesis modification that minimize aggregation and intro-



duce small molecules or ions have enabled the development of fluorescent pDA-based materials. For instance, polydopamine-glutathione nanoparticles synthesized *via* Michael addition between dopamine and reduced glutathione (GSH) displayed significantly stronger fluorescence than conventional pDA NPs prepared under similar conditions.<sup>167</sup> Moreover, the controlled addition of hydrogen peroxide during synthesis further optimized particle formation and emission intensity.<sup>167</sup> Unlike pDA, which requires post-processing or chemical modifications to become fluorescent, pLD NPs naturally exhibit photoluminescence. As demonstrated by Hormozi-Nezhad *et al.*, the fluorescence emission of pLD nanoparticles is excitation-dependent, with a maximum emission observed at 419 nm when excited at 340 nm.<sup>168</sup> These optical properties were instrumental in developing a fluorescence-based sensor for the detection of L-DOPA itself, a key neurotransmitter used in Parkinson's disease management. The assay achieved a low detection limit of 29 nM and a strong linear response between 0.3–100  $\mu\text{M}$ , offering a simple and cost-effective alternative to existing detection methods.<sup>168</sup> Similarly, pNE NPs have been exploited to detect their corresponding neurotransmitter, norepinephrine, using their intrinsic fluorescence.<sup>169</sup> Under alkaline conditions, norepinephrine was oxidized *in situ* to fluorescent pNE nanoparticles with intense green emission around 527 nm upon excitation at 365 nm; these nanoparticles serve as the reporting element of a probe for norepinephrine in urine, achieving a detection limit of 49 nM with a linear response over 0–40  $\mu\text{M}$ .<sup>169</sup> pEP has also shown strong potential in optical biosensing, particularly in the form of fluorescent NPs. pEP can form fluorescent organic dots (pEP-FODs) with intrinsic emission properties. In a study by Gao *et al.*, pEP-FODs exhibited a defined HOMO–LUMO structure (–7.31 eV and –3.91 eV, respectively) and a bandgap of 3.4 eV, making them highly responsive to metal-ion quenching.<sup>75</sup> This photoluminescence is quenched upon interaction with  $\text{Fe}^{3+}$  ions *via* a photoinduced electron transfer mechanism.<sup>75</sup> Gerelkhuu *et al.* further illustrated this process as involving the 3d orbitals of  $\text{Fe}^{3+}$ , which accept electrons from the conduction band of pEP-coated nanoparticles during bioimaging.<sup>76</sup> They demonstrated selective fluorescence quenching in the presence of  $\text{Fe}^{3+}$  ions.<sup>76</sup>

Building on this quenching-based behaviour, polydopamine also functions as an effective fluorescence quencher, often *via* Förster resonance energy transfer (FRET).<sup>170</sup> Its broad UV-visible absorption and weak intrinsic emission make it an excellent acceptor. In a recent example, Xue *et al.* developed dendritic fibrous silica nanoparticles functionalized with pDA that demonstrated high quenching efficiency, exceeding 95% after just two hours of dopamine polymerization.<sup>171</sup> The pDA layer strongly adsorbs (primarily *via*  $\pi$ – $\pi$  stacking with nucleobases) and quenches fluorophore probes.<sup>171</sup> Moreover, pDA's quenching capacity extends beyond its role as a coating and can also function as the primary nanomaterial. Polydopamine nanospheres, for instance, were used to quench DNA probes in a dual nucleases-assisted cyclic amplification approach for miRNA detection, enabling signal amplification

without PCR.<sup>172</sup> Similar platforms have been developed from poly-L-DOPA, where dendritic pLD NPs were used for dye-labelled single stranded DNA.<sup>173</sup> These systems achieved high quenching, up to 96.1%, comparable to pDA based platforms, *via* a combination of  $\pi$ – $\pi$  stacking between exposed nucleobases and the aromatic pLD network, modulated by electrostatic repulsion and ionic strength.<sup>173</sup> By contrast, analogous quenching-based biosensors have not yet been systematically reported for pNE. However, cells cultured on pNE-coated displayed attenuated DAPI fluorescence, similar to what is observed on pDA coating,<sup>79</sup> suggesting that catechol-rich conjugated structures in pNE also promote strong fluorescence quenching. This comparable quenching behaviour remains largely unexplored in the context of pNE-based optical biosensing applications.

In addition to its intrinsic fluorescence and quenching properties, pDA is also valued in fluorescence biosensors for its easily functionalizable surface, which enables stable immobilization of various fluorophores. Compared to conventional immobilisation based on 1-ethyl-3-(3-(dimethylamino)propyl)carbo-diimide hydrochloride/*N*-hydroxysulfosuccinimide (EDC/NHS) chemistry, the pDA-functionalized sensors exhibited higher antigen binding and lower detection limits.<sup>174</sup> Moreover, fluorescently labeled antibodies were immobilized directly onto pDA-coated gold surfaces to enhance sensitivity.<sup>175</sup> Under controlled coating condition (1–5 nm thickness), pDA-coated gold achieved a detection limit of 1.0 pM, outperforming conventional uncoated gold surfaces functionalized with alkanethiol self-assembled monolayers, which reached a detection limit of 4 pM.<sup>175</sup> This increase in sensitivity is not restricted to surface coatings: pDA NPs increased the refractive index sensitivity of a fiber optic SPR biosensor by 55.7% compared to the unmodified one.<sup>176</sup> Notably, pLD has also been employed to enhance optical detection performance. Its value lies in its adhesive surface chemistry and rich functionalization potential, which enable higher biomolecule loading and efficient loading interactions.<sup>177,178</sup> For example, He *et al.* employed pLD NPs as colorimetric labels in lateral flow immunoassays (LFIA) for SARS-CoV-2 and influenza detection.<sup>178</sup> The abundant carboxylic acid groups on the pLD surface enabled strong covalent attachment of antibodies, and the resulting pLD-LFIA reached a detection limit of 5  $\text{pg mL}^{-1}$  for SARS-CoV-2 antigen and 0.1  $\text{ng mL}^{-1}$  for influenza A H1N1, showing higher sensitivity than gold nanoparticle-based LFIAs.<sup>178</sup>

Lastly, polycatecholamines also act as powerful platforms for SERS signal amplification. pDA's adhesive and reductive properties also facilitate the construction of highly sensitive and reusable SERS biosensors.<sup>8</sup> Its reductive nature enables the *in situ* synthesis and uniform deposition of noble metal NPs, creating localized surface plasmon 'hot spots' critical for electromagnetic enhancement. In addition, pDA's aromatic and  $\pi$ -rich structure promotes strong  $\pi$ – $\pi$  stacking and covalent interactions with target analytes or Raman reporters, enhancing chemical adsorption and signal amplification within complex nanostructures.<sup>8</sup> Similarly, several studies have



demonstrated that pLD-mediated metal reduction enables the formation of uniform and reproducible SERS substrates, where the catechol and carboxylic acid groups promote nanoparticle nucleation, stabilization, and hot spot generation.<sup>179,180</sup> These properties result in sensitive and selective Raman detection, extending the versatility of pLD from bio-interfaces into the domain of optical biosensors. Given that SERS performance is driven by the same metal-chelating and reducing mechanisms described above, comparable platforms based on pNE and pEP have, to date, scarcely been explored, underscoring a clear opportunity for future biosensors development.

**Outlook.** pDA remains the most widely adopted polycatecholamine for biosensing, particularly in electrochemical and optical sensor platforms. Its high surface adhesion and redox reactivity, which is driven by catechol-to-quinone conversion and the potential formation of DHI units, support the stable immobilization of enzymes, aptamers, nanoparticles, and antibodies on electrode surfaces. These structural features enable strong  $\pi$ - $\pi$  stacking, covalent conjugation *via* quinones, and redox signal enhancement. pDA has been successfully integrated into devices for detecting different biomarkers, glucose, dopamine, miRNAs.<sup>149,155,172,181</sup> However, it is also known for fluorescence quenching, limiting its utility in optical biosensors unless coupled with spacers or fluorophore-compatible matrices.

On the other hand, pLD has emerged as a promising electrochemical and optical sensing platform, primarily due to its carboxyl group, which enhances the anchoring of enzymes, antibodies, and charged analytes through electrostatic or covalent interactions. Studies have shown that pLD-based biosensors can achieve higher sensitivities and better enzyme retention than their pDA counterpart, particularly for glucose oxidase.<sup>156</sup> This suggests its superior capacity for biofunctional entrapment, and points toward broader utility in immobilizing nucleic acids, aptamers, or redox-active peptides. Nonetheless, the number of published electrochemical platforms using pLD remains limited, and its broader application in label-free detection is still underdeveloped.

pNE offers a unique profile for optical and surface-enhanced sensing, owing to its  $\beta$ -hydroxyl group and its ability to form ultrasoft coatings. These structural features support enhanced hydrogen bonding and minimal background signal,<sup>182</sup> making pNE well-suited for fluorescence-based biosensors and metal-enhanced formats like SERS. pNE's chelation capacity<sup>163</sup> indicates potential for ion-detection or catalytic transduction mechanisms. Although it has been successfully integrated mostly into SPR-MIP hybrid systems,<sup>145-148</sup> its broader use in fluorescence or multiplexed biosensing remains largely untapped. The antifouling and conformal properties of pNE coatings may be particularly valuable for *in vivo* or wearable sensor platforms, where signal clarity and biocompatibility are critical.

pEP, though generally less cohesive in film-forming behavior due to its secondary amine and lack of DHI formation, has shown surprisingly strong promise in biosensing applications. Its oxidative chemistry yields fluorescent intermediates like

adrenochrome and adrenolutin, which introduce inherent redox activity and optical responsiveness. Notably, pEP-based photoelectrochemical biosensors have outperformed those built on pDA and pNE, with higher photocurrents and improved analytical stability.<sup>153</sup> These results suggest that, despite its lower structural integrity, pEP can serve as a versatile platform for fluorescence- and redox-active biosensors, particularly if functionalized with specific molecular probes or redox reporters. Furthermore, its fluorescent behavior under metal ion coordination, such as  $\text{Fe}^{3+}$  quenching,<sup>75,76</sup> opens the door for reusable, nanoparticle-integrated sensing formats, yet to be fully explored.

### Drug delivery

Drug delivery systems aim to enhance the therapeutic efficacy and safety of pharmaceutical compounds by controlling their release and by targeting specific tissues. Traditional administration routes, such as oral or parenteral, often lead to systemic distribution, rapid clearance, and potential damage to non-target organs. For example, oral absorption is especially challenging for proteins and peptides due to poor bioavailability, while high systemic doses are often required to achieve therapeutic concentrations at the target site.<sup>183</sup> To address these limitations, research has increasingly focused on nanoparticle-based platforms, which offer controlled release, improved drug loading, and site-specific delivery. These capabilities are enabled by tuning the size, morphology, and surface chemistry of the carrier.<sup>184</sup>

Among polycatecholamines, polydopamine has been extensively exploited as a morphologically versatile nanocarrier. pDA nanoparticles can be engineered into various shapes of variable complexity, each providing distinct advantages for drug delivery applications (Fig. 7A).<sup>7,184</sup> These morphologies can be tailored by modifying synthesis parameters, including dopamine concentration, solvent composition, reaction temperature, and stirring speed.<sup>7,111,191</sup> Mesoporous pDA nanoparticles, for instance, are often synthesized using soft-template methods involving surfactants such as Pluronic F127 and swelling agents like 1,3,5-trimethylbenzene (TMB).<sup>111,191</sup> This nanoemulsion approach promotes  $\pi$ - $\pi$  stacking interactions during polymerization, producing structured pores that enhance drug loading and enable controlled release profiles. Adjusting the TMB-to-F127 ratio enables the transition from solid to hollow mesoporous structures, thereby optimizing cavity size for drug encapsulation.<sup>185</sup> In addition, hollow pDA nanoparticles, prepared by coating removable templates such as silica or emulsions followed by core dissolution, provide internal cavities capable of high-capacity drug encapsulation.<sup>186</sup> Alternatively, soft-template methods employing dimethyldiethoxysilane emulsion droplets enable precise shell thickness and capsule size control without harsh chemical treatments.<sup>7</sup> Anisotropic pDA nanoparticles, including bowl-shaped and walnut-shaped structures, have been synthesized *via* interfacial polymerization or anisotropic assembly processes, and demonstrate improved cellular uptake compared to spherical particles.<sup>187,188</sup> This enhancement arises from



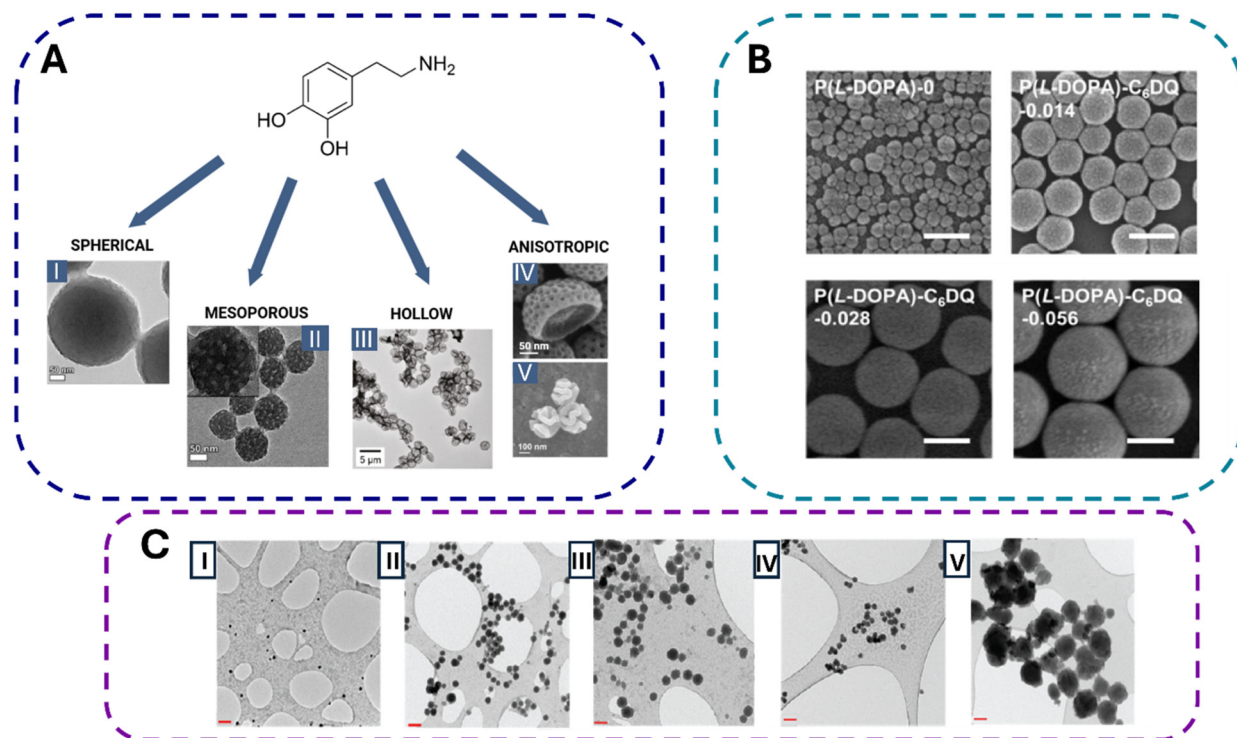


**Fig. 7** Morphological diversity of pDA NPs synthesized from dopamine, demonstrating the tunability of their structure. (A) Depending on the synthesis conditions, pDA NPs can form distinct architectures including (I) spherical, (II) mesoporous, (III) hollow, (IV) anisotropic like bowl-shaped, and (V) walnut-shaped structures. Panel (I) and (II) adapted with permission from ref. 185. Copyright 2016 American Chemical Society. Panel (III) adapted with permission from ref. 186 (<https://pubs.acs.org/doi/10.1021/cm201390e>). Further permissions related to the material excerpted should be directed to the ACS. Panel (IV) adapted from ref. 187. Copyright 2016 American Chemical Society. Panel (V) adapted with permission from ref. 188. Copyright 2018 Wiley. (B) Representative SEM images of pLD nanoparticles prepared without (P(L-DOPA) – 0) and with increasing amounts of the double-headed quaternary ammonium cross-linker C6DQ. Scale bars = 250 nm. Adapted from ref. 189. Copyright 2024 American Chemical Society. (C) TEM images of pNE nanoparticles synthesized under varying monomer and ethanol concentrations: (I) 2.5 mM monomer in 2.8 mM ethanol, (II) 4.5 mM monomer in 2.8 mM ethanol, (III) 6 mM monomer in 2.8 mM ethanol, (IV) 6 mM monomer in 5.6 mM ethanol, (V) 6 mM monomer in 0.1 mM ethanol. Adapted with permission from ref. 190. Copyright 2020 Royal Society of Chemistry.

increased cell membrane contact and favorable endocytic pathways. In fact, bowl-shaped mesoporous pDA nanoparticles (~210 nm diameter, ~8 nm mesopores) exhibited significantly enhanced internalization rates over spherical counterparts.<sup>187</sup>

pNE has also emerged as a promising material for drug delivery platforms, both as coatings for NPs to enhance drug loading<sup>192</sup> and as nanoparticles themselves.<sup>163,190,193</sup> In contrast to pDA, for which complex internal architectures and non-spherical shapes are actively engineered, current work on polynorepinephrine has primarily focused on controlling particle dimension rather than morphology, since this feature is critical for controlling cellular uptake, biodistribution, and therapeutic release. This tunability can be achieved through various synthetic strategies, including metal ion chelation,<sup>163</sup> solvent modulation,<sup>190</sup> and precursor concentration control.<sup>190</sup> pNE metal ion chelation properties were leveraged to synthesize metal-doped nanoparticles with different diameters.<sup>163</sup> These metal-doped pNE nanoparticles exhibited diameters ranging from around 70 to 500 nm, dependent on the specific metal ions employed (*e.g.*, Fe<sup>3+</sup>, Mg<sup>2+</sup>, Co<sup>2+</sup>).<sup>163</sup> Another synthesis approach involved variations in solvent composition,

particularly the amount of ethanol, further modulating nanoparticle dimensions from approximately 157 nm to 495 nm.<sup>190</sup> Higher ethanol content yielded smaller and more uniform particles, indicating precise morphological control *via* solvent adjustment (Fig. 7C).<sup>190</sup> Additionally, varying norepinephrine concentration independently allowed further control over particle dimensions, ranging approximately from 130 to 346 nm.<sup>190</sup>

The development of pLD as a nanocarrier in drug delivery began considerably later than pDA, with the first reported application emerging in 2018.<sup>194</sup> Compared to other polycatecholamines, pLD nanoparticles appear intrinsically biased toward relatively small diameters under simple auto-oxidation conditions, with a typical range of diameter 50–60 nm (ref. 113, 189 and 195) with very low mass yields (2–3 wt%).<sup>113,189</sup> This has been attributed to insufficient physical aggregation during growth,<sup>189</sup> likely linked to the high density of carboxylic groups which weakens noncovalent stacking. Notably, size and yield can be effectively increased by strengthening these physical cross-links. In water, as shown in Fig. 7B, introducing the double-headed quaternary ammonium molecule C<sub>6</sub>DQ pro-



motes stronger intermolecular associations, increasing NP diameters to several hundred nanometres and raising yields from ~3 wt% up to ~60 wt%.<sup>189</sup> Similarly, coordination with metal ions such as Zn<sup>2+</sup> or Mn<sup>2+</sup> produces larger pLD (120–160 nm) increasing the amount of dopant and with substantially higher yields.<sup>113,196</sup> Also, varying the synthesis temperature (at fixed amount of Zn content) showed that thermal control is an effective strategy.<sup>113</sup> Specifically, increasing the reaction temperature from 30 °C to 75 °C nearly doubled NP diameter (from ~70 to ~150 nm) and increased the yield by roughly five-fold, a stronger effect than that achieved by simple increasing the amount of Zn dopant.<sup>113</sup>

Despite the rich chemical reactivity and biocompatibility of pEP, its application in drug delivery and nanocarrier systems remains strikingly underexplored when compared to other polycatecholamines. Very few studies have reported the successful formation of well-defined pEP-based NPs, and this may in part be attributed to the limited fundamental work on its self-assembly behavior. The diverse morphologies observed in pEP systems<sup>75,190</sup> (from fluorescent organic dots to crystalline lamellae) can be rationalized through the buffer-dependent aggregation model proposed by Hu *et al.*<sup>25</sup> Their study demonstrated that redox conditions, pH, and buffer composition critically influence epinephrine's oxidation kinetics, intermediate stabilization, and final aggregate morphology.<sup>25</sup> This helps explain why different synthesis conditions yield vastly different results. For instance, when epinephrine was polymerized in strongly alkaline NaOH (pH ~ 11) at an elevated temperature (60 °C), it formed small, uniform fluorescent nanoparticles (~2–4 nm in diameter).<sup>75</sup> In contrast, using a water–ethanol mixture at mild alkaline pH resulted in petal-like microstructures (~0.8–1 μm wide and 4–5 μm long).<sup>67</sup> In another study, Lu *et al.* attempted to synthesize NPs using Tris buffer with ethanol, but found that no particles formed at pH 8.5.<sup>190</sup> Only at a higher pH of 9.7 they observed sheet-like crystalline aggregates, highlighting the importance of surpassing a critical oxidation threshold.<sup>190</sup> This aligns with Hu *et al.*'s finding that Tris can inhibit polymer stacking, suggested to arise from covalent interaction with quinone intermediates.<sup>25</sup> Such high sensitivity to environmental conditions may be a major factor limiting the standardization and reproducibility of pEP nanostructures for biomedical use.

While particle size and morphology control biodistribution and cellular uptake, the surface chemistry largely dictates drug-loading capacity, stability, and interactions with biological barriers. Owing to their inherent biocompatibility and ease of surface functionalization, pDA nanoparticles possess abundant catechol, amine, and quinone groups. These groups facilitate high drug loading *via* π–π stacking, hydrogen bonding, and electrostatic interactions.<sup>53</sup> As a result, pDA NPs typically carry a negative surface charge at physiological pH, which helps prolong circulation time by minimizing nonspecific protein adsorption.<sup>184</sup> However, this negative charge can also enhance opsonization and internalization by macrophages potentially limiting their cellular uptake efficiency.<sup>184</sup> Therefore, surface modifications such as PEGylation are com-

monly employed to reduce nanoparticle surface negativity. This creates a steric barrier against immune recognition, thereby minimizing opsonization and further extending blood circulation.<sup>197</sup> Analogous design principles apply to polynorepinephrine NPs, which have also been PEGylated to improve systemic circulation and *in vivo* tumor accumulation. Similar to pDA, pNE contains abundant catechol and amine functionalities, which enable efficient drug loading *via* π–π stacking, hydrogen bonding, and electrostatic interactions with therapeutic molecules.<sup>190,192</sup> However, pNE-based systems exhibit superior drug-loading capacity compared to pDA analogues prepared under similar conditions. In the study by Liu *et al.*, PEGylated pNE NPs reached a drug loading of doxorubicin (DOX) of 67.7% markedly higher than the 42% measured for pDA.<sup>193</sup> This improvement was attributed to the lower zeta potential of pNE-PEG, which favors electrostatic adsorption of positively charged DOX.<sup>193</sup> As shown in Fig. 8B, flow cytometry further showed that cells treated with pNE NPs internalized approximately 1.9-fold more DOX than those exposed to pDA NPs, and fluorescence microscopy revealed much stronger nuclear DOX signal.<sup>193</sup> Moreover, multiple studies have confirmed its low cytotoxicity profile both *in vitro* and *in vivo*.<sup>163,190</sup> Specifically, pNE nanoparticles demonstrated minimal toxicity toward HeLa cells and zebrafish embryos even at concentrations up to 500 μg mL<sup>-1</sup>, confirming their excellent cytocompatibility and systemic safety.<sup>190</sup> In the case of pLD, surface chemistry introduces complementary advantages arising from its carboxylated side chains. In this first reported application, pLD was used as a surface coating on Fe<sub>3</sub>O<sub>4</sub> nanoparticles for magnetically guided delivery of paclitaxel in breast cancer treatment.<sup>194</sup> The polymer's adhesive catechol backbone, coupled with its acid-stable carboxylic side chains, conferred superior environmental stability compared to pDA.<sup>194</sup> Moreover, the pLD-coated nanocomposites enabled a more uniform and sustained drug release over 24 hours, demonstrating improved release control relative to earlier pDA systems.<sup>194</sup> The carboxyl groups of pLD, absent in pDA, provide accessible sites for covalent peptide conjugation and enhance electrostatic interactions with drug molecules, leading to greater drug-loading capacities, improved dispersion in aqueous media, and selective tumor accumulation *in vivo*.<sup>198,199</sup>

The surface chemistry also governs their stimuli-response behaviour. In the case of pDA, under acidic conditions, the protonation of amines can promote pH-triggered drug release.<sup>184,200</sup> The responsiveness of pDA nanoparticles to acidic environments has been particularly exploited in cancer treatments, given the inherently acidic nature of tumor tissues compared to healthy counterparts. For instance, loading the chemotherapeutic drug DOX onto pDA nanoparticles resulted in a formulation that remained highly stable at neutral pH (7.0), with less than 5% of DOX being released over 48 hours.<sup>201</sup> In contrast, under acidic conditions (pH 5.0) representative of endolysosome environments, a significant burst release of DOX was observed.<sup>201</sup> A similar pH responsiveness has been reported for pNE systems. At acidic pH levels



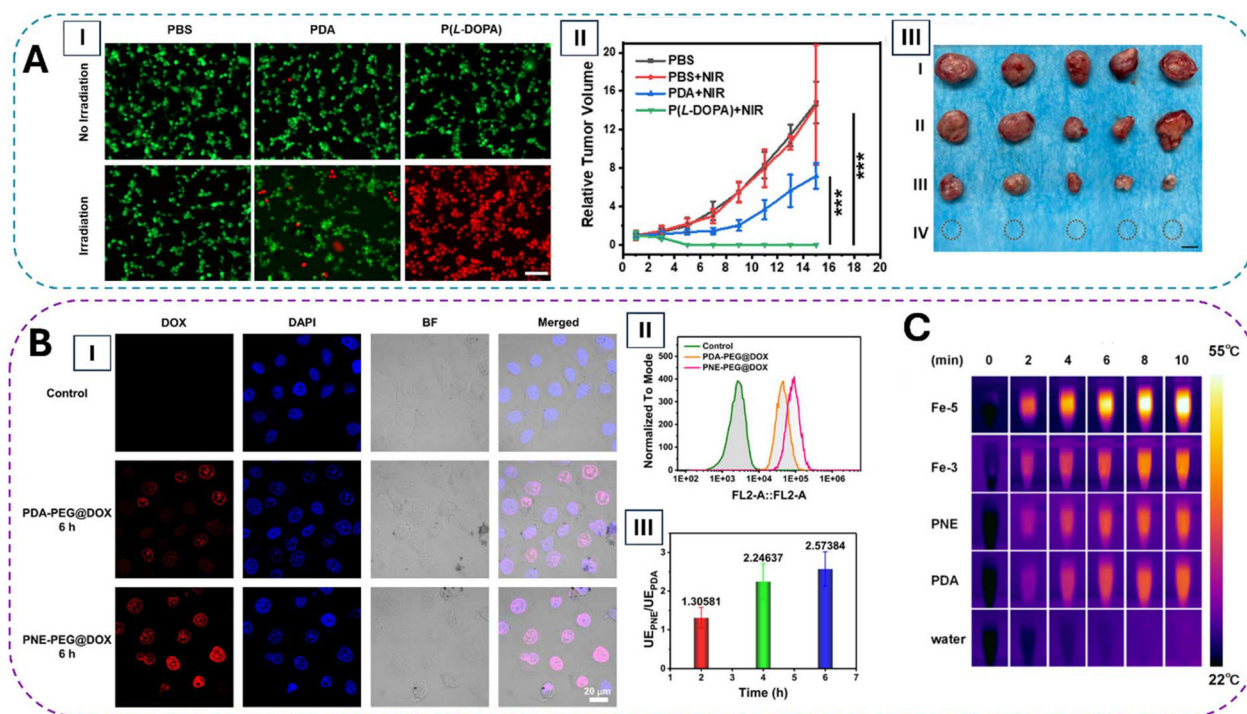


**Fig. 8** (A) (I) Fluorescence images of CT26 cells treated with PBS, pDA NPs, or pLD NPs with or without NIR irradiation (808 nm,  $1.5 \text{ W cm}^{-2}$  for 3 min), stained with Calcein-AM (live cells, green) and PI (dead cells, red). Scale bar =  $20 \mu\text{m}$ . (II) Normalized tumor growth curves for tumor-bearing mice treated with PBS, PBS + NIR, pDA + NIR, and pLD (P(L-DOPA)) + NIR; tumor volume was recorded every 2 days after photothermal treatment. (III) Representative photographs of tumors excised at the end of the study for the four groups: I, PBS; II, PBS + NIR; III, pDA + NIR; IV, pLD + NIR. Scale bar = 1 cm. Adapted with permission from ref. 189. Copyright 2024 American Chemical Society. (B) (I) Confocal laser scanning microscopy (CLSM) images of HeLa cells after 6 h incubation with pDA-PEG@DOX or pNE-PEG@DOX nanoparticles; blue indicates DAPI-stained nuclei and red indicates DOX fluorescence (scale bar =  $20 \mu\text{m}$ ). (II) Flow cytometry histograms of cellular DOX uptake for control, pDA-PEG@DOX, and pNE-PEG@DOX. (III). Ratio of cellular uptake efficiency (UE) of pNE-PEG-FITC to pDA-PEG-FITC nanoparticles at different incubation times. Adapted with permission from ref. 193. Copyright 2019 American Chemical Society. (C) Photothermal imaging of water, pDA, pNE, Fe-3, and Fe-5 dispersions under 808 nm laser irradiation ( $1.5 \text{ W cm}^{-2}$ ) over 10 min. Adapted with permission from ref. 163. Copyright 2024 American Chemical Society.

( $\sim 5.0$ ), pNE undergoes amine protonation and disruption of  $\pi$ - $\pi$  stacking, weakening drug-nanoparticle interactions and promoting drug release.<sup>190,192,193</sup> In contrast, at neutral pH, minimal release is observed, preserving drug integrity during systemic circulation.<sup>192,193</sup> These properties have been successfully leveraged in cancer therapy models. For example, Lu *et al.* loaded DOX into pNE nanoparticles and obtained a clear pH-dependent release profile: at pH 5.0, the cumulative DOX release reached  $\sim 90\%$  after 24 hours, whereas only  $\sim 40\%$  of the drug was released over the same period at pH 7.4.<sup>190</sup> Consistent with this release behaviour, DOX-loaded pNE NPs enhanced cytotoxicity in HeLa cells than free DOX, reflecting both enhanced cellular uptake and preferential drug release under acidic, tumour-like conditions.<sup>190</sup>

Moreover, polycatecholamines NPs has also shown efficient photothermal properties, they can convert NIR light into heat for minimally invasive cancer therapy. Traditional cancer therapies, including surgery, radiotherapy, and chemotherapy, often suffer from low specificity, leading to systemic toxicity and limited efficacy, while nanomaterial-based systems, such as pDA nanoparticles, offer a promising alternative by enabling

targeted and multifunctional treatment modalities.<sup>202</sup> For example, dopamine-melanin colloidal nanospheres synthesized by Liu *et al.* achieved a photothermal conversion efficiency of approximately 40%, effectively transforming NIR irradiation into localized heat for rapid and precise tumor ablation *in vivo*, without damaging surrounding healthy tissues.<sup>203</sup> pNE NPs also exhibit strong photothermal conversion efficiency upon NIR irradiation.<sup>163,193</sup> Liu *et al.* reported a photothermal efficiency of  $\sim 51.2\%$ , which exceeds that of pDA-based analogues ( $\sim 42\%$ ) and surpasses many conventional agents such as gold nanoparticles and polypyrrole.<sup>193</sup> Compared to pDA, pNE exhibits a narrower HOMO-LUMO gap (1.36 eV vs. 1.80 eV), facilitating electron excitation and heat generation under NIR light (Fig. 8C).<sup>163</sup> This results in improved intramolecular charge transfer and more efficient conversion of light into heat. The additional  $\beta$ -hydroxyl group in pNE likely enhances  $\pi$ -conjugation and electron delocalization, contributing to this narrowed bandgap and higher photothermal output.<sup>163</sup> Similarly, pLD NPs have also demonstrated enhanced photothermal properties compared to pDA. As shown in Fig. 8A, Wang *et al.* developed quaternary



ammonium-assisted pLD nanoparticles that achieved a photothermal conversion efficiency of 25.5%, approximately 55% higher than that of pDA (~16.5%).<sup>189</sup> This enhancement was attributed to the higher DHICA content in pLD, which red shifts NIR absorption due to auxochromic effects of the carboxyl group, and allows for improved light harvesting and heat conversion.<sup>189</sup> Notably, *in vivo* pLD NPs induced a larger temperature increase at the tumour side under irradiation and completely inhibited tumour growth, with no recurrence observed over 15-day period; whereas pDA NPs at the same dose and laser conditions only partially suppressed tumour growth<sup>189</sup> (Fig. 8A).

The strong photothermal response and rich coordination chemistry of polycatecholamines have been extensively exploited also in combination therapies, where photothermal heating is coupled with chemotherapy or other modalities. For example, the adhesive properties of pDA nanoparticles make them well-suited as nanocarriers in combination therapies involving chemotherapy and photothermal treatments.<sup>204,205</sup> Similarly, pNE-coated FeOOH nanoparticles loaded with artemisinin demonstrated a remarkable efficacy.<sup>192</sup> Under NIR light, this system completely eliminated tumors *in vivo*, with no recurrence after 30 days, ultimately underscoring the high efficacy of pNE-based combination therapies.<sup>192</sup> pLD has also been incorporated into multimodal cancer therapies.<sup>189,196</sup> Kang *et al.* introduced Mn<sup>2+</sup>-doped pLD nanoparticles carrying both DOX and pheophorbide A for a trimodal cancer therapy combining chemotherapy, photothermal therapy, and photodynamic therapy.<sup>196</sup> Crucially, the catechol and carboxyl moieties in pLD acted as high-affinity chelation sites, enabling a Mn<sup>2+</sup> loading of 28.2 wt%, in stark contrast to just 0.08 wt% observed in equivalent pDA-based systems.<sup>196</sup> The incorporation of Mn<sup>2+</sup> not only boosted T1-weighted MRI contrast but also acted as a co-factor enhancing photothermal effects.<sup>196</sup> Additionally, the pLD-based particles reached a photothermal conversion efficiency of 87.6%, more than double that of conventional pDA.<sup>196</sup> These combined properties resulted in more potent tumor ablation under NIR irradiation, without sacrificing biocompatibility.<sup>196</sup> More recently, pEP has recently been implemented in a theranostic nanocarrier platform for cancer treatment. In a 2025 study, Lee *et al.* developed a core-shell nanoparticle system composed of a perfluorocarbon (PFC) core coated with a fluorescent pEP shell (pEPP) chelated with Fe<sup>2+</sup> ions.<sup>206</sup> These PFC@pEPP-Fe nanoparticles were engineered to provide dual-mode imaging (fluorescence and ultrasound) and synergistic photothermal/chemodynamic therapy.<sup>206</sup> Upon NIR light activation, the pEP shell converted light into heat, triggering oxygen release from the PFC core and promoting hydroxyl radical generation.<sup>206</sup> The system demonstrated strong tumor specificity, imaging capabilities, and therapeutic efficacy *in vivo*.<sup>206</sup> This work represents one of the first successful demonstration of pEP as a multifunctional nanocarrier and highlights its untapped potential in drug delivery and cancer nanomedicine.

In addition to their application in oncology, polycatecholamine nanoparticles (particularly pDA and pLD) have shown

significant potential in inflammatory bowel, autoimmune, and central nervous system (CNS) disorders.<sup>111,113,195,207–209</sup> Central to these broader biomedical applications is pDA's dual functionality: its excellent drug-loading capabilities, and its intrinsic antioxidant activity which derives from abundant catechol groups that efficiently scavenge ROS,<sup>99,100</sup> thus mitigating oxidative stress and inflammation. In autoimmune and inflammatory diseases such as rheumatoid arthritis and inflammatory bowel disease, excessive ROS production exacerbates inflammation and tissue damage. pDA nanoparticles counteract this by reducing oxidative stress, and subsequent tissue injury.<sup>111,207</sup> Additionally, their high drug-loading capacity enables effective delivery of anti-inflammatory drugs, further enhancing therapeutic outcomes.<sup>111</sup> Lastly, in CNS disorders, such as Parkinson's and Alzheimer's diseases, oxidative stress and neuroinflammation are key drivers of neuronal damage and degeneration. pDA nanoparticles have shown promise in crossing biological barriers, including the blood-brain barrier, delivering therapeutic agents directly to the brain.<sup>208</sup> Their intrinsic antioxidant activity provides neuroprotective effects by reducing oxidative damage and inflammation, offering potential therapeutic advantages for neurodegenerative conditions.<sup>208</sup> However, the comparative studies discussed above indicate that pDA is not necessarily the optimal polycatecholamine in every context. Similarly to pDA, pLD scavenges ROS *via* its redox-active catechol and quinone groups.<sup>113,209</sup> Moreover, Wang *et al.* showed that ZnO-assisted pLD nanoparticles, with ~90% DHICA content, outperform pDA due to their looser microstructure, higher HOMO levels, and lower oxidation potential.<sup>113</sup> These structural features enabled pLD to achieve a substantially lower EC<sub>50</sub> in ABTS and DPPH assays, translating to greater antioxidant properties.<sup>113</sup> pLD demonstrates a potent antioxidant and anti-inflammatory properties, making it a promising candidate for treating inflammatory and autoimmune diseases.<sup>113,209</sup> Furthermore, pLD's therapeutic relevance extends to the central nervous system.<sup>195</sup> Levodopa remains the gold standard treatment for Parkinson's disease, yet its systemic administration often leads to motor complications and off-target toxicity.<sup>18</sup> In this context, NanoDOPA micelles composed of amphiphilic PEG-*b*-poly(L-DOPA) block copolymers were developed for the gradual release of L-DOPA *in vivo via* enzymatic hydrolysis, allowing sustained and localized delivery.<sup>195</sup> Compared to free L-DOPA, NanoDOPA improved behavioral outcomes and significantly reduced dyskinesia in Parkinsonian mice, offering a more controlled and side-effect-sparing alternative to conventional systemic therapy.<sup>195</sup>

**Outlook.** pDA has been widely explored in drug delivery applications, due to its catechol-driven redox activity, pH responsiveness, and ability to form diverse nanostructures. Various morphologies, such as nanospheres, nanobowls, hollow capsules, and porous aggregates, have been developed to enhance drug loading efficiency, release kinetics, and targeting capabilities, particularly for tumor therapy. Its catechol groups also allow it to scavenge ROS, offering additional therapeutic benefit in oxidative-stress-related diseases.



**Table 1** Comparative performance of polycatecholamine derivatives (pLD, pNE, pEP) relative to pDA across key surface and functional properties. Y = outperforms pDA; N = no demonstrated advantage over pDA; U.E. = underexplored

Property	pLD vs. pDA	pNE vs. pDA	pEP vs. pDA
Thinner coating	Y <sup>63</sup>	Y <sup>63</sup>	U.E.
Smoother coating	Y <sup>22</sup>	Y <sup>38</sup>	Y <sup>35,153</sup>
Greater hydrophilicity	Y <sup>63,214</sup>	Y <sup>38,63,214</sup>	N <sup>35</sup>
Better bioconjugation	Y <sup>156</sup>	Y <sup>89,215</sup>	U.E.
Improved pH stability	Y <sup>22</sup>	Y <sup>215</sup>	U.E.
Photothermal properties	Y <sup>113,189</sup>	Y <sup>163</sup>	U.E.
Hemocompatibility	Y <sup>63</sup>	Y <sup>63</sup>	U.E.
Immunomodulatory activity	N <sup>63</sup>	Y <sup>63</sup>	U.E.
Antioxidant properties	Y <sup>113</sup>	U.E.	U.E.
Antibacterial properties	U.E.	Y <sup>132</sup>	U.E.
Antifouling properties	U.E.	Y <sup>132</sup>	U.E.
Drug loading properties	U.E.	Y <sup>193</sup>	U.E.
<b>Potential new application</b>	pH-Responsive drug delivery	Bioadhesive for inflamed wounds	Smooth coatings for neural interfaces

By comparison, pLD, pNE, and pEP remain significantly underexplored in the context of structural control and functionalized delivery. Lu *et al.* demonstrated that mesoporous and anisotropic nanoparticles, including nanobowls and nanogolf balls, can be successfully synthesized from pNE and pEP, using a modified soft-templating method.<sup>210</sup> These structures showed enhanced performance in photoacoustic imaging, and by extension, hold promise for improved drug encapsulation and uptake.<sup>210</sup> However, such shape–function investigations remain extremely limited compared to the wealth of data available for pDA, indicating a need for broader exploration of morphological tuning in pLD-, pNE-, and pEP-based systems.

In terms of chemical functionality, pLD's carboxyl group provides a natural advantage for pH-sensitive drug release, a feature particularly advantageous in the acidic tumor micro-environment. Yet, despite this capability, the application of pLD in stimuli-responsive or targeted nanocarriers remains nascent. Likewise, pNE shares the catechol moiety of pDA, suggesting it could also possess ROS-scavenging capacity, a property that has not yet been directly investigated and it has already shown lower inflammatory response compared to pDA.<sup>63</sup> Together, these properties make pNE a particularly attractive candidate for inflammatory or neuroprotective delivery context, where tissues experience chronic oxidative and immune stress, and a low additional inflammatory burden is essential.

Studies have explored incorporating gene therapy and therapeutic cancer vaccines into pDA-based nanoparticle platforms, significantly enhancing treatment outcomes beyond conventional chemotherapy.<sup>211–213</sup> pDA has been used to immobilize DNA, RNA, and protein antigens through a combination of covalent and noncovalent interactions while preserving their biological activity. Given that pLD and pNE coatings have already been shown to be compatible with biomacromolecules and maintain cell viability, their higher hydrophilicity and reduced fouling behaviour could be exploited to design next-generation nucleic-acid and vaccine carriers with improved stability and controlled immune activation. The presence of carboxylic groups in pLD offers additional anchoring sites for cationic gene complexes or protein antigens, while the milder inflammatory profile of pNE may help limit off-target immune

responses. Take together these features suggest that pLD- and pNE-based platforms could be optimal gene and vaccine delivery system, even though studies are still scarce.

pEP, although showing structural stability in nanogolf-ball forms and inherent fluorescent behavior, remains the least studied polycatecholamine for drug delivery. Its adreno-chrome-based oxidation intermediates may provide unique opportunities for theranostic tracking, yet no systematic studies exist on its loading capacity, biodistribution, or *in vivo* clearance.

## Conclusion and perspectives

Polydopamine has long stood as the gold-standard polycatecholamine in biomedical engineering, delivering a remarkably simple yet powerful platform for surface modification, bioadhesion, sensing and drug delivery. However, as this perspective illustrates, pDA represents only one point on a much broader chemical landscape. The emergence of pNE, pLD and pEP reveals a family of polymers whose distinct side-chain functionalities fundamentally reshape polymerization kinetics, coating morphology, redox activity and biological response, offering distinctive advantages in specific biomedical contexts (Table 1). Together, these materials show that catecholamine-derived polymers are a modular chemical toolkit with properties that can be predictively tuned to the needs of specific biomedical environments.

Yet despite their promise, the field is still in its early stages. One of the clearest messages emerging from the current literature is the paucity of structural knowledge. Despite the large body of work on polydopamine, its precise molecular architecture remains under debate, a challenge that is even more pronounced for pNE, pLD, and pEP. Moving forward, progress will depend on integrating high-resolution characterization techniques and computational modelling to establish structure–function relationships that can guide rational material design rather than empirical trial-and-error.

Developing such design rules also requires systematic, head-to-head comparisons under identical polymerization con-



ditions. Today, results are difficult to compare because coating thickness, oxidant choice, pH, ionic strength and buffer identity vary widely across studies. A unified experimental framework would allow direct benchmarking across all four polymers. Such standardization would enable the field to progress from descriptive observations to quantitative guidelines for application-specific solutions.

Beyond fundamental chemistry, the future of polycatecholamines also lies in their integration into next-generation biomedical technologies. Their tunable hydrophilicity, adhesion chemistry, redox reactivity, and metal-chelation capacity make them natural candidates for smart or stimuli-responsive systems. Likewise, their compatibility with technologies such as 3D printing, microfluidics, organ-on-chip platforms, and wearable biosensors positions these polymers as enabling materials for preclinical technologies.

In particular, a critical frontier will lay in understanding biodegradation pathways and the bioactivity of degradation products. The discovery that pDA's degradation chemistry influences biological outcomes in unexpected ways warrants similar studies with pNE, pLD, and pEP, whose degradation products may also interact with specific cellular pathways. Mapping this will be essential for evaluating long-term biocompatibility, especially for implants, biodegradable scaffolds and nanocarriers designed for *in vivo* use. In this context, the long-term metabolic fate of polycatecholamine-coated systems remains poorly understood. Most studies have focused on the *in vitro* performance or short-term animal experiments, but critical information regarding their biodistribution, degradation pathways, and clearance mechanisms is still lacking. Emilsson *et al.* demonstrated that even PEGylated polycatecholamine-coated nanocrystals, including those made with pDA and pNE, were subject to rapid clearance from circulation and significant liver accumulation despite high PEG grafting densities.<sup>216</sup> This behavior was linked to the formation of a fibrogen-enriched protein corona, suggesting that strong interactions with cysteine-rich plasma proteins may override conventional PEG stealth effects.<sup>216</sup> While this study offers a systematic look at polycatecholamine-coated nanoparticle clearance, it also underscores a broader issue: the structural heterogeneity and insufficient characterization of these polymers prevent reliable predictions of their *in vivo* stability, enzymatic degradation, and long-term biocompatibility. More comprehensive pharmacokinetic and clearance studies, particularly involving macroscopic coatings and non-nanoparticle formats, are urgently needed to support the translation of polycatecholamine materials into clinically approved delivery systems.

While substantial progress has been made, polycatecholamine-based materials still face significant obstacles in their path to clinical translation, primarily due to structural ambiguities and limited understanding of their long-term biological interactions and clearance pathways. To date, the only dopamine derived polycatecholamine system that has entered human testing is SYNT-101,<sup>217</sup> a gastrointestinal “synthetic epithelial lining” based on the platform developed by Li

*et al.*<sup>218</sup> In this strategy, orally administered dopamine polymerizes in the catalase and H<sub>2</sub>O<sub>2</sub> rich proximal small intestine, creating a transient polydopamine-like coating on the mucosa that redirects nutrient adsorption and can act as a local carrier for macromolecular drugs.<sup>218</sup> However, this first-in-human evaluation of SYNT-101, reported to date only as a conference abstract, involved nine healthy volunteers who each received a single oral dose at one of three dose levels, with endoscopic and histological assessment at 24 h and biochemical follow-up over 10 days. While this pilot provides proof of duodenal coverage and short-term safety, it remains a very preliminary dataset and falls far short of the evidence required for regulatory approval or widespread clinical use.<sup>217</sup> Moving forward, a concerted effort in structural characterization, systematic studies on polymerization conditions, and comprehensive *in vivo* evaluations are crucial to bridge the gap between laboratory research and clinical applicability. Addressing these challenges will not only enhance the biomedical impact of polycatecholamines but also pave the way for their integration into innovative therapeutic, diagnostic, and regenerative solutions.

In conclusion, the polycatecholamine family represents a rich but underexploited chemical space. Moving beyond the dopamine-centric view that has shaped the past fifteen years, the field now stands on the threshold of a much broader and more sophisticated toolkit. By integrating advanced structural characterization, standardized comparative studies and application-driven optimization, researchers can begin to leverage each polymer's unique chemistry. Doing so will unlock new opportunities across tissue engineering, regenerative medicine, biosensing and drug delivery, ultimately positioning polycatecholamines as a class of well-established bioinspired materials rather than isolated curiosity-driven alternatives branching from polydopamine.

## Conflicts of interest

The authors declare no conflict of interest.

## Data availability

No primary research results, software or code have been included and no new data were generated or analysed as part of this review.

## Acknowledgements

This work was supported by the Natural Sciences and Engineering Research Council of Canada (NSERC) through the Discovery grant (RGPIN-2020-05945). Permission has been obtained for all reused figures. Copyright acknowledgments are included in the figure captions as required.



## References

- M. Mehdizadeh and J. Yang, *Macromol. Biosci.*, 2013, **13**, 271–288.
- N. Pandey, L. F. Soto-Garcia, J. Liao, P. Zimmern, K. T. Nguyen and Y. Hong, *Biomater. Sci.*, 2020, **8**, 1240–1255.
- P. Kord Forooshani and B. P. Lee, *J. Polym. Sci., Part A: Polym. Chem.*, 2017, **55**, 9–33.
- P. M. Costa, D. A. Learmonth, D. B. Gomes, M. P. Cautela, A. C. N. Oliveira, R. Andrade, J. Espregueira-Mendes, T. R. Veloso, C. B. Cunha and R. A. Sousa, *Polymers*, 2021, **13**, 3317.
- H. Lee, S. M. Dellatore, W. M. Miller and P. B. Messersmith, *Science*, 2007, **318**, 426–430.
- M. K. Yazdi, M. Zare, A. Khodadadi, F. Seidi, S. M. Sajadi, P. Zarrintaj, A. Arefi, M. R. Saeb and M. Mozafari, *ACS Biomater. Sci. Eng.*, 2022, **8**, 2196–2219.
- S. Acter, M. Moreau, R. Ivkov, A. Viswanathan and W. Ngwa, *Nanomaterials*, 2023, **13**, 1656.
- L. Tian, C. Chen, J. Gong, Q. Han, Y. Shi, M. Li, L. Cheng, L. Wang and B. Dong, *Sensors*, 2023, **23**, 4641.
- M. Sugumaran and J. J. Evans, *J. Funct. Biomater.*, 2023, **14**, 449.
- R. Laverty, *Drugs*, 1978, **16**, 418–440.
- T. G. Barclay, H. M. Hegab, S. R. Clarke and M. Ginic-Markovic, *Adv. Mater. Interfaces*, 2017, **4**, 1601192.
- M. E. Gnegy, in *Basic Neurochemistry: Principles of Molecular, Cellular, and Medical Neurobiology*, ed. D. L. P. Scott T. Brady, G. J. Siegel and R. Wayne Albers, Academic Press, Elsevier, Eighth., 2011, pp. 283–299.
- J. Motiejunaite, L. Amar and E. Vidal-Petiot, *Ann. Endocrinol.*, 2021, **82**, 193–197.
- A. P. Strafella, T. Paus, M. Fraraccio and A. Dagher, *Brain*, 2003, **126**, 2609–2615.
- D. S. Goldstein, in *eLS*, John Wiley & Sons, Ltd, 2010, pp. 1–9.
- F. Elmadjian, J. M. Hope and E. T. Lamson, *J. Clin. Endocrinol. Metab.*, 1957, **17**, 608–620.
- J. A. Myburgh, A. Higgins, A. Jovanovska, J. Lipman, N. Ramakrishnan and J. Santamaria, *Intensive Care Med.*, 2008, **34**, 2226–2234.
- J. A. Borovac, *Yale J. Biol. Med.*, 2016, **89**, 37–47.
- M. K. Sung, J. Rho, I. S. Choi, P. B. Messersmith and H. Lee, *J. Am. Chem. Soc.*, 2009, **131**, 13224–13225.
- J. Kuang, J. L. Guo and P. B. Messersmith, *Adv. Mater. Interfaces*, 2014, **1**, 1400145.
- A. Petran, R. Mrówczyński, C. Filip, R. Turcu and J. Liebscher, *Polym. Chem.*, 2015, **6**, 2139–2149.
- H. Wei, J. Ren, B. Han, L. Xu, L. Han and L. Jia, *Colloids Surf., B*, 2013, **110**, 22–28.
- M. Gaeta, R. Randazzo, V. Villari, N. Micali, A. Pezzella, R. Purrello, M. D'Ischia and A. D'Urso, *Front. Chem.*, 2020, **8**, 616961.
- R. Mrówczyński, R. Markiewicz and J. Liebscher, *Polym. Int.*, 2016, **65**, 1288–1299.
- L. Hu, N. Gao, J. Shan, X. Wang, H. Wang, X. Yang, H. Ma and Q. Wei, *Langmuir*, 2020, **36**, 5040–5047.
- H. Jeong and S. Hong, *ACS Appl. Polym. Mater.*, 2024, **6**, 14158–14168.
- M. Dai, L. Sun, L. Chao, Y. Tan, Y. Fu, C. Chen and Q. Xie, *ACS Appl. Mater. Interfaces*, 2015, **7**, 10843–10852.
- L. C. Almeida, R. D. Correia, B. Palys, J. P. Correia and A. S. Viana, *Electrochim. Acta*, 2021, **386**, 138515.
- A. M. Jaramillo, R. Barrera-Gutiérrez and M. T. Cortés, *ACS Omega*, 2020, **5**, 15016–15027.
- R. Abdel-Hamid and E. F. Newair, *J. Electroanal. Chem.*, 2013, **704**, 32–37.
- W. Cheng, X. Zeng, H. Chen, Z. Li, W. Zeng, L. Mei and Y. Zhao, *ACS Nano*, 2019, **13**, 8537–8565.
- J. Y. Kim, W. I. Kim, W. Youn, J. Seo, B. J. Kim, J. K. Lee and I. S. Choi, *Nanoscale*, 2018, **10**, 13351–13355.
- M. Dai, T. Huang, L. Chao, Q. Xie, Y. Tan, C. Chen and W. Meng, *Talanta*, 2016, **149**, 117–123.
- L. Liu, C. Chen, C. Chen, X. Kang, H. Zhang, Y. Tao, Q. Xie and S. Yao, *Talanta*, 2019, **194**, 343–349.
- C. Dhand, S. Harini, M. Venkatesh, N. Dwivedi, A. Ng, S. Liu, N. K. Verma, S. Ramakrishna, R. W. Beuerman, X. J. Loh and R. Lakshminarayanan, *ACS Appl. Mater. Interfaces*, 2016, **8**, 1220–1232.
- S. Li, H. Wang, M. Young, F. Xu, G. Cheng and H. Cong, *Langmuir*, 2019, **35**, 1119–1125.
- H. Hemmatpour, O. De Luca, D. Crestani, M. C. A. Stuart, A. Lasorsa, P. C. A. van der Wel, K. Loos, T. Giousis, V. Haddadi-Asl and P. Rudolf, *Nat. Commun.*, 2023, **14**, 664.
- S. Hong, J. Kim, Y. S. Na, J. Park, S. Kim, K. Singha, G. Im, D. Han, W. J. Kim and H. Lee, *Angew. Chem.*, 2013, **125**, 9357–9361.
- J. Liebscher, R. Mrowczynski, H. A. Scheidt, C. Filip, N. D. Hadade, R. Turcu, A. Bende and S. Beck, *Langmuir*, 2013, **29**, 10539–10548.
- J. H. Ryu, P. B. Messersmith and H. Lee, *ACS Appl. Mater. Interfaces*, 2018, **10**, 7523–7540.
- J. Liebscher, *Eur. J. Org. Chem.*, 2019, 4976–4994.
- Y. Liu, K. Ai and L. Lu, *Chem. Rev.*, 2014, **114**, 5057–5115.
- Z. Lu, B. M. Teo and R. F. Tabor, *J. Mater. Chem. B*, 2022, **10**, 7895–7904.
- M. Ischia, K. Wakamatsu, S. Briganti, D. Kovacs, P. Meredith, A. Pezzella, T. Sarna, J. D. Simon and S. Ito, *Pigm. Cell Melanoma Res.*, 2013, **26**, 616–633.
- G. Marcelo, M. D. M. López-González, M. Vega and C. Pecharromán, *Nanomaterials*, 2021, **11**, 2320.
- Y. T. Liu, T. M. Lee and T. S. Lui, *Colloids Surf., B*, 2013, **106**, 37–45.
- M. Fornal, A. Krawczyńska and A. Belcarz, *ACS Appl. Mater. Interfaces*, 2024, **16**, 40515–40530.
- M. A. Ivanova, E. K. Nefedova, E. M. Mal'tseva, A. V. Kalensii and A. A. Zvekov, *J. Appl. Spectrosc.*, 2022, **89**, 905–912.
- M. D'Ischia, A. Napolitano, A. Pezzella, E. J. Land, C. A. Ramsden and P. A. Riley, in *Advances in Heterocyclic*



- Chemistry*, Academic Press, Elsevier, 2005, vol. 89, pp. 1–63.
- 50 R. P. Bacil, P. H. M. Garcia and S. H. P. Serrano, *J. Electroanal. Chem.*, 2022, **908**, 116111.
- 51 R. A. Heacock, in *Advances in Heterocyclic Chemistry*, Academic Press, Elsevier, 1965, vol. 5, pp. 205–290.
- 52 M. D'Ischia, A. Palumbo and G. Prota, *Tetrahedron*, 1988, **44**, 6441–6446.
- 53 J. Yang, M. A. Cohen Stuart and M. Kamperman, *Chem. Soc. Rev.*, 2014, **43**, 8271–8298.
- 54 N. F. Della Vecchia, R. Avolio, M. Alfè, M. E. Errico, A. Napolitano and M. D'Ischia, *Adv. Funct. Mater.*, 2013, **23**, 1331–1340.
- 55 D. R. Dreyer, D. J. Miller, B. D. Freeman, D. R. Paul and C. W. Bielawski, *Langmuir*, 2012, **28**, 6428–6435.
- 56 W. Chan, *Rapid Commun. Mass Spectrom.*, 2019, **33**, 429–436.
- 57 Y. Ding, L.-T. Weng, M. Yang, Z. Yang, X. Lu, N. Huang and Y. Leng, *Langmuir*, 2014, **30**, 12258–12269.
- 58 H. A. Lee, Y. Ma, F. Zhou, S. Hong and H. Lee, *Acc. Chem. Res.*, 2019, **52**, 704–713.
- 59 Q. Lyu, N. Hsueh and C. L. L. Chai, *ACS Biomater. Sci. Eng.*, 2019, **5**, 2708–2724.
- 60 C. J. Wilson, R. E. Clegg, D. I. Leavesley and M. J. Percy, *Tissue Eng.*, 2005, **11**, 1–18.
- 61 H. Wang, C. Lin, X. Zhang, K. Lin, X. Wang and S. G. Shen, *ACS Appl. Mater. Interfaces*, 2019, **11**, 7615–7625.
- 62 J. Yan, R. Wu, S. Liao, M. Jiang and Y. Qian, *Front. Bioeng. Biotechnol.*, 2020, **8**, 590998.
- 63 X. Tan, P. Gao, Y. Li, P. Qi, J. Liu, R. Shen, L. Wang, N. Huang, K. Xiong, W. Tian and Q. Tu, *Bioact. Mater.*, 2021, **6**, 285–296.
- 64 M. Ni, J. C. M. Teo, M. S. bin Ibrahim, K. Zhang, F. Tasnim, P. Y. Chow, D. Zink and J. Y. Ying, *Biomaterials*, 2011, **32**, 1465–1476.
- 65 Y. J. Kim, G. M. Park, W. K. Cho and D. H. Woo, *ACS Chem. Neurosci.*, 2024, **15**, 4132–4142.
- 66 S. M. Kim, M. S. Lee, J. Jeon, D. H. Lee, K. Yang, S. W. Cho, I. Han and H. S. Yang, *Macromol. Biosci.*, 2018, **18**, 1800290.
- 67 V. O. Kollath, M. Derakhshandeh, F. D. Mayer, T. Mudigonda, M. N. Islam, M. Trifkovic and K. Karan, *RSC Adv.*, 2018, **8**, 31967–31971.
- 68 S. H. Ku, J. Ryu, S. K. Hong, H. Lee and C. B. Park, *Biomaterials*, 2010, **31**, 2535–2541.
- 69 S. H. Ku and C. B. Park, *Biomaterials*, 2010, **31**, 9431–9437.
- 70 G. Jin, H. Huang, X. Bao and S. P. Palecek, *ACS Biomater. Sci. Eng.*, 2024, **10**, 7429–7440.
- 71 X. Jiang, Y. Li, Y. Liu, C. Chen and M. Chen, *RSC Adv.*, 2016, **6**, 60206–60214.
- 72 M. Park, M. Shin, E. Kim, S. Lee, K. I. Park, H. Lee and J. H. Jang, *J. Nanomater.*, 2014, **2014**, 793052.
- 73 S. M. Kang and H. Lee, *Bull. Korean Chem. Soc.*, 2013, **34**, 960–962.
- 74 S. Khetani, K. W. Yong, V. O. Kollath, E. Eastick, M. Azarmanesh, K. Karan, A. Sen and A. Sanati-Nezhad, *ACS Appl. Mater. Interfaces*, 2020, **12**, 6910–6923.
- 75 Z. F. Gao, T. T. Li, X. L. Xu, Y. Y. Liu, H. Q. Luo and N. B. Li, *Biosens. Bioelectron.*, 2016, **83**, 134–141.
- 76 Z. Gerelkhuu, B. T. Huy, D. Jung, M. Sharipov and Y. I. Lee, *Anal. Bioanal. Chem.*, 2021, **413**, 1363–1371.
- 77 A. J. Steeves, A. Atwal, S. C. Schock and F. Variola, *J. Mater. Chem. B*, 2016, **4**, 3145–3156.
- 78 T. Nardo, V. Chiono, G. Ciardelli and M. Tabrizian, *Macromol. Biosci.*, 2016, **16**, 288–298.
- 79 P. Kowalczyk, K. Kopeć, M. Wojasiński, J. Jaroszewicz and T. Ciach, *Biomater. Adv.*, 2023, **151**, 213489.
- 80 L. Li, Y. Li, L. Yang, F. Yu, K. Zhang, J. Jin, J. Shi, L. Zhu, H. Liang, X. Wang and Q. Jiang, *Ann. Transl. Med.*, 2019, **7**, 240.
- 81 R. Toita, J. Sunarso, A. N. Rashid, K. Tsuru and K. Ishikawa, *J. Mater. Chem. B*, 2015, **3**, 8738–8746.
- 82 G. Tan, Y. Liu, Y. Wu, K. Ouyang, L. Zhou, P. Yu, J. Liao and C. Ning, *Electrochim. Acta*, 2017, **228**, 343–350.
- 83 C. Kao, C. Lin, Y. Chen, C. Yeh, H. Fang and M. Shie, *Mater. Sci. Eng., C*, 2015, **56**, 165–173.
- 84 H. Yang, Y. Xu, M. Zhu, Y. Gu, W. Zhang, H. Shao, Y. Wang, Z. Ping, X. Hu, L. Wang and D. Geng, *Biomaterials*, 2016, **80**, 1–10.
- 85 J. Gong, C. Ye, J. Ran, X. Xiong, X. Fang, X. Zhou, Y. Yi, X. Lu, J. Wang, C. Xie and J. Liu, *ACS Nano*, 2023, **17**, 16573–16586.
- 86 T. Ma, C. X. Wang, X. Y. Ge and Y. Zhang, *Macromol. Biosci.*, 2023, **23**, 2300067.
- 87 J. S. Lee, J. Lee and J. S. Heo, *J. Cell Commun. Signaling*, 2018, **12**, 661–672.
- 88 B. M. Protein-, A. W. G. Nijhuis, J. J. J. P. Van Den Beucken, O. C. Boerman, J. A. Jansen and S. C. G. Leeuwenburgh, *Tissue Eng., Part C*, 2013, **19**, 610–619.
- 89 D. Yang, X. Wang, Q. Ai, J. Shi and Z. Jiang, *RSC Adv.*, 2015, **5**, 42461–42467.
- 90 J. Kang, S. Tada, T. Kitajima, T. I. Son, T. Aigaki and Y. Ito, *BioMed Res. Int.*, 2013, **2013**, 265980.
- 91 Y. Yang, Y. Zhang, R. Chai and Z. Gu, *Front. Bioeng. Biotechnol.*, 2020, **8**, 616.
- 92 C. Chen, J. Yu, H.-Y. Ng, A.-X. Lee, C.-C. Chen, Y. Chen and M. Shie, *Materials*, 2018, **11**, 1665.
- 93 M. B. Taskin, R. Xu, H. Zhao, X. Wang, M. Dong, F. Besenbacher and M. Chen, *Phys. Chem. Chem. Phys.*, 2015, **17**, 9446–9453.
- 94 C.-H. Chen, C.-C. Tsai, P.-T. Wu, I.-K. Wang, J. Yu and W.-B. Tsai, *Appl. Bio Mater.*, 2019, **2**, 205–216.
- 95 S. H. Bhang, S. H. Kwon, S. Lee, G. C. Kim, A. M. Han, Y. H. K. Kwon and B. S. Kim, *Biochem. Biophys. Res. Commun.*, 2013, **430**, 1294–1300.
- 96 Y. Qian, X. Zhao, Q. Han, W. Chen, H. Li and W. Yuan, *Nat. Commun.*, 2018, **9**, 323.
- 97 L. Zhou, J. Ge, M. Wang, M. Chen, W. Cheng, W. Ji and B. Lei, *Bioact. Mater.*, 2021, **6**, 1605–1617.
- 98 J. F. Rocha, L. H. Hasimoto and M. Santhiago, *Anal. Bioanal. Chem.*, 2023, **415**, 3799–3816.
- 99 K. Y. Ju, Y. Lee, S. Lee, S. B. Park and J. K. Lee, *Biomacromolecules*, 2011, **12**, 625–632.



- 100 X. Bao, J. Zhao, J. Sun, M. Hu and X. Yang, *ACS Nano*, 2018, **12**, 8882–8892.
- 101 S. H. Ku and C. B. Park, *Adv. Healthcare Mater.*, 2013, **2**, 1445–1450.
- 102 Y. Liu, G. Zhou, Z. Liu, M. Guo, X. Jiang, M. B. Taskin, Z. Zhang, J. Liu, J. Tang, R. Bai, F. Besenbacher, M. Chen and C. Chen, *Sci. Rep.*, 2017, **7**, 8197.
- 103 A. Michalicha, A. Espona-Noguera, C. Canal, B. Budzyńska, M. Pięt, S. Przywara, J. Pawelec and A. Belcarz, *Biomater. Adv.*, 2022, **133**, 112645.
- 104 A. Michalicha, C. Canal, A. Espona-Noguera, M. Piet, B. Budzyńska, S. Przywara and A. Belcarz, *Int. J. Mol. Sci.*, 2022, **23**, 9369.
- 105 C. Sperling, M. F. Maitz, S. Grasso, C. Werner and S. M. Kanse, *Appl. Mater. Interfaces*, 2017, **9**, 40107–40116.
- 106 W. Tsai, W. Chen, H. Chien, W. Kuo and M. Wang, *Acta Biomater.*, 2011, **7**, 4187–4194.
- 107 Y. Cai, J. Li, K. Poh, C. Tan, S. Thian, J. Y. Fuh, J. Sun, B. Y. Tay and W. Wang, *J. Mater. Chem. B*, 2013, **1**, 5971–5976.
- 108 X. Ren, J. Li, J. Li, Y. Jiang, L. Li, Q. Yao, Q. Ke and H. Xu, *Chem. Eng. J.*, 2019, **370**, 1027–1038.
- 109 P. Chen, S. Wang, Z. Huang, Y. Gao, Y. Zhang, C. Wang, T. Xia, L. Li, W. Liu and L. Yang, *J. Mater. Sci. Technol.*, 2021, **70**, 91–104.
- 110 Y. Zhang, L. Lu, Y. Chen, J. Wang, Y. Chen, C. Mao and M. Yang, *Biomater. Sci.*, 2019, **7**, 5232–5237.
- 111 M. Wu, C. Hong, C. Shen, D. Xie, T. Chen, A. Wu and Q. Li, *Drug Delivery*, 2023, **30**, 2289846.
- 112 S. Zhao, M. Fang, Y. Li, F. Wang, H. Li and L. Wang, *Biomater. Sci.*, 2023, **11**, 6504–6523.
- 113 X. Wang, J. Zhang, L. Yang, T. Wang, G. Duan, Z. Gu and Y. Li, *Biomacromolecules*, 2024, **25**, 2563–2573.
- 114 W. Duan, X. Bian and Y. Bu, *Front. Bioeng. Biotechnol.*, 2021, **9**, 716035.
- 115 J. Park, Y. Kim, B. Chun and J. Seo, *Biotechnol. J.*, 2021, **16**, 2100231.
- 116 V. Dhandapani, V. Ringuette, M. Desrochers, M. Sirois and P. Vermette, *J. Biomed. Mater. Res., Part B*, 2022, **110**, 2779–2797.
- 117 K. Zheng, Q. Gu, D. Zhou, M. Zhou and L. Zhang, *Smart Mater. Med.*, 2022, **3**, 41–65.
- 118 S. Tavakoli, H. Mokhtari, M. Kharaziha, A. Kermanpur, A. Talebi and J. Moshtaghian, *Mater. Sci. Eng., C*, 2020, **111**, 110837.
- 119 H. Montazerian, A. Hassani Najafabadi, E. Davoodi, R. Seyedmahmoud, R. Haghniaz, A. Baidya, W. Gao, N. Annabi, A. Khademhosseini and P. S. Weiss, *Adv. Healthcare Mater.*, 2023, **12**, 2203404.
- 120 C. Ghobril and M. W. Grinstaff, *Chem. Soc. Rev.*, 2015, **44**, 1820–1835.
- 121 H. An, Z. Gu, L. Zhou, S. Liu, C. Li, M. Zhang, Y. Xu, P. Zhang and Y. Wen, *Acta Biomater.*, 2022, **149**, 126–138.
- 122 N. R. de Barros, A. Gangrade, A. Rashad, R. R. Chen, F. Zehtabi, M. Ermis, N. Falcone, R. Haghniaz, S. Khosravi, A. Gomez, S. Huang, M. Mecwan, D. Khorsandi, J. Lee, Y. Zhu, B. Li, H. J. Kim, F. G. Thankam and A. Khademhosseini, *Acta Biomater.*, 2024, **173**, 231–246.
- 123 M. Li, Z. Zhang, Y. Liang, J. He and B. Guo, *ACS Appl. Mater. Interfaces*, 2020, **12**, 35856–35872.
- 124 H. Liu, Q. Li, Y. Xu, Y. Sun, X. Fan, H. Fang, B. Hu, L. Huang, L. Liao and X. Wang, *Biomater. Sci.*, 2023, **11**, 3180–3196.
- 125 N. Pandey, L. Soto-Garcia, S. Yaman, A. Kuriakose, A. U. Rivera, V. Jones, J. Liao, P. Zimmern, K. T. Nguyen and Y. Hong, *Biomater. Adv.*, 2022, **134**, 112589.
- 126 Y. M. Gao, Z. Y. Li, X. J. Zhang, J. Zhang, Q. F. Li and S. B. Zhou, *ACS Appl. Mater. Interfaces*, 2023, **15**, 11496–11506.
- 127 Y. Y. Yeh, Y. Y. Lin, T. T. Wang, Y. J. Yeh, T. H. Chiu, R. Wang, M. Y. Bai and Y. C. Yeh, *Acta Biomater.*, 2023, **170**, 344–359.
- 128 A. Michalicha, A. Roguska, A. Przekora, B. Budzyńska and A. Belcarz, *Carbohydr. Polym.*, 2021, **272**, 118485.
- 129 J. H. Kim, J. I. Lim and H. K. Park, *J. Porous Mater.*, 2013, **20**, 177–182.
- 130 J. I. Lim, J. H. Kim and H. K. Park, *Mater. Lett.*, 2012, **81**, 251–253.
- 131 H. Montazerian, A. Baidya, R. Haghniaz, E. Davoodi, S. Ahadian, N. Annabi, A. Khademhosseini and P. S. Weiss, *ACS Appl. Mater. Interfaces*, 2021, **13**, 40290–40301.
- 132 Z. Lu, A. J. Quek, S. P. Meaney, R. F. Tabor, B. Follink and B. M. Teo, *ACS Appl. Bio Mater.*, 2020, **3**, 5880–5886.
- 133 Y. Fu, L. Yang, J. Zhang, J. Hu, G. Duan, X. Liu, Y. Li and Z. Gu, *Mater. Horiz.*, 2021, **8**, 1618–1633.
- 134 L. Huan, H. Tan, J. Song, M. Lei, E. Kim, G. F. Payne and C. Liu, *Acta Biomater.*, 2019, **88**, 181–196.
- 135 Y. Ye, L. Zheng, T. Wu, X. Ding, F. Chen, Y. Yuan, G. C. Fan and Y. Shen, *ACS Appl. Mater. Interfaces*, 2020, **12**, 35626–35637.
- 136 C. Yang, X. Ma, P. Wu, L. Shang, Y. Zhao and L. Zhong, *Small*, 2023, **19**, 2301092.
- 137 F. Cheng, L. Xu, X. Zhang, J. He, Y. Huang and H. Li, *Int. J. Biol. Macromol.*, 2024, **260**, 129372.
- 138 C. Zhang, L. Xiang, J. Zhang, C. Liu, Z. Wang, H. Zeng and Z. K. Xu, *Chem. Sci.*, 2022, **13**, 1698–1705.
- 139 L. Peng, Y. Liang, J. Yue, H. Li, A. Deng, S. Xie, X. Z. Tang, J. Wang and Z. Mao, *RSC Adv.*, 2023, **13**, 3635–3642.
- 140 P. Mehrotra, *J. Oral Biol. Craniofacial Res.*, 2016, **6**, 153–159.
- 141 N. Bisht, N. Dwivedi, A. Khosla, D. P. Mondal, A. K. Srivastava and C. Dhand, *J. Electrochem. Soc.*, 2022, **169**, 107505.
- 142 M. Zandieh, B. M. Hagar and J. Liu, *Part. Part. Syst. Charact.*, 2020, **37**, 2000208.
- 143 A. Lamaoui, A. A. Lahcen and A. Amine, *Polymers*, 2023, **15**, 3712.
- 144 N. F. El Azab, A. M. Mahmoud and Y. A. Trabik, *J. Electroanal. Chem.*, 2022, **918**, 116504.
- 145 F. Torrini, P. Palladino, V. Baldoneschi, S. Scarano and M. Minunni, *Anal. Chim. Acta*, 2021, **1161**, 338481.



- 146 D. Sestaioni, W. Giurlani, G. Ciacci, V. Camagni, P. Palladino, A. Barucci and S. Scarano, *Anal. Chim. Acta*, 2024, **1321**, 343037.
- 147 V. Baldoneschi, P. Palladino, M. Banchini, M. Minunni and S. Scarano, *Biosens. Bioelectron.*, 2020, **157**, 112161.
- 148 F. Torrini, G. Ferraro, E. Fratini, P. Palladino, S. Scarano and M. Minunni, *Biosens. Bioelectron.*, 2024, **252**, 116133.
- 149 F. Xie, Y. Zhou, X. Liang, K. Wu, Z. Zhou, M. Bao, J. Zhang, J. Luo, S. Liu and J. Ma, *J. Electrochem. Soc.*, 2021, **168**, 077514.
- 150 M. S. Alhumaidi, F. Arshad, C. Aubry, F. Ravaux, J. Mcelhinney, A. Hasan and L. Zou, *Nanotechnology*, 2020, **31**, 275602.
- 151 Z. Xu, R. Han, N. Liu, F. Gao and X. Luo, *Sens. Actuators, B*, 2020, **319**, 128253.
- 152 C. Jeon, J. H. Byeon, E. Park, S. Kim, S. Kim and W. K. Cho, *Langmuir*, 2025, **41**, 1099–1106.
- 153 H. Ma, Q. Fan, B. Fan, Y. Zhang, D. Fan, D. Wu and Q. Wei, *Langmuir*, 2018, **34**, 7744–7750.
- 154 M. Sensi, G. Migatti, V. Beni, T. M. D'Alvise, T. Weil, M. Berto, P. Greco, C. Imbriano, F. Biscarini and C. A. Bortolotti, *Macromol. Mater. Eng.*, 2022, **307**, 2100880.
- 155 V. Fedorenko, D. Damberga, K. Grundsteins, A. Ramanavicius, S. Ramanavicius, E. Coy, I. Iatsunskyi and R. Viter, *Polymers*, 2021, **13**, 2918.
- 156 M. Dai, T. Huang, L. Chao, Y. Tan, C. Chen, W. Meng and Q. Xie, *RSC Adv.*, 2016, **6**, 17016–17022.
- 157 V. Baldoneschi, P. Palladino, S. Scarano and M. Minunni, *Anal. Bioanal. Chem.*, 2020, **412**, 5945–5954.
- 158 Y. Liu, X. Nan, W. Shi, X. Liu, Z. He, Y. Sun and D. Ge, *RSC Adv.*, 2019, **9**, 16439–16446.
- 159 A. Jędrzak, M. Kuznowicz, T. Rębiś and T. Jesionowski, *Bioelectrochemistry*, 2022, **145**, 108071.
- 160 A. Jędrzak, M. Kuznowicz, K. Hoffa and T. Jesionowski, *J. Appl. Electrochem.*, 2025, **55**, 1519–1532.
- 161 N. Bisht, M. Patel, N. Dwivedi, P. Kumar, D. P. Mondal, A. K. Srivastava and C. Dhand, *Environ. Res.*, 2023, **227**, 115684.
- 162 M. Chaturvedi, M. Patel, D. P. Mondal, A. K. Srivastava, N. Dwivedi and C. Dhand, *Electrochim. Acta*, 2024, **475**, 143630.
- 163 J. Yuan, Y. Liu, Y. Li, Q. Chang, X. Deng and Y. Xie, *Nano Lett.*, 2024, **24**, 6353–6361.
- 164 T. K. Das, S. Remanan, S. Ghosh, S. K. Ghosh and N. C. Das, *Environ. Nanotechnol., Monit. Manage.*, 2021, **15**, 100411.
- 165 J. Sun, Q. Ma, D. Xue, W. Shan, R. Liu, B. Dong, J. Zhang, Z. Wang and B. Shao, *Trends Anal. Chem.*, 2021, **140**, 116273.
- 166 A. Menichetti, A. Mavridi-Printezi, D. Mordini and M. Montalti, *Biosensors*, 2023, **13**, 956.
- 167 L. Tang, S. Mo, S. G. Liu, N. Li, Y. Ling, N. B. Li and H. Q. Luo, *Sens. Actuators, B*, 2018, **259**, 467–474.
- 168 M. R. Hormozi-Nezhad, A. Moslehipour and A. Bigdeli, *Sens. Actuators, B*, 2017, **243**, 715–720.
- 169 M. A. Farahmand, F. Ghasemi and M. R. Hormozi-nezhad, *Anal. Chim. Acta*, 2018, **1039**, 124–131.
- 170 C. Biskup, T. Zimmer, L. Kelbauskas, B. Hoffmann, N. Klöcker, W. Becker, A. Bergmann and K. Benndorf, *Microsc. Res. Tech.*, 2007, **70**, 442–451.
- 171 X. Xue, H. Persson and L. Ye, *Microchim. Acta*, 2024, **191**, 180.
- 172 D. Huang, P. Shen, C. Xu, Z. Xu, D. Cheng, X. Zhu, M. Fang, Z. Wang and Z. Xu, *Biosens. Bioelectron.*, 2023, **222**, 114957.
- 173 J. Liu, C. Zou, C. Chen, H. Fang, Q. Wu, H. Yu, J. Zhu, L. Li, S. Yang and W. Huang, *Talanta*, 2020, **219**, 121285.
- 174 S. Shi, L. Wang, R. Su, B. Liu, R. Huang, W. Qi and Z. He, *Biosens. Bioelectron.*, 2015, **74**, 454–460.
- 175 M. Toma and K. Tawa, *Jpn. J. Appl. Phys.*, 2018, **57**, 03EK01.
- 176 G. Cao, P. Chang, A. Zhang, F. Liu, H. Pan, J. Wang, S. Lin and T. Yang, *Opt. Fiber Technol.*, 2023, **80**, 103468.
- 177 L. Liu, Y. Jia, S. Jin, X. Chen and P. Zhou, *Microchem. J.*, 2023, **192**, 108947.
- 178 K. He, Y. Ye, S. Liu, P. Yuan, W. Sun and J. Tang, *Biochem. Biophys. Res. Commun.*, 2024, **709**, 149821.
- 179 B. Calis and M. Yilmaz, *Colloids Surf., A*, 2021, **622**, 126654.
- 180 H. Mazlumoglu and M. Yilmaz, *Phys. Chem. Chem. Phys.*, 2021, **23**, 13396–13404.
- 181 S. Bakshi, K. Li, P. Dong, I. Barth, C. Kunstmann-Olsen, S. Johnson and T. F. Krauss, *Talanta*, 2024, **268**, 125300.
- 182 V. O. Kollath, V. P. K. Venu, M. Saifeddine, K. Mihara, S. A. Hirota, M. D. Hollenberg and K. Karan, *Nanoscale Adv.*, 2024, **7**, 830–839.
- 183 N. Zahin, R. Anwar, D. Tewari, M. T. Kabir, A. Sajid, B. Mathew, M. S. Uddin, L. Aleya and M. M. Abdel-Daim, *Environ. Sci. Pollut. Res.*, 2020, **27**, 19151–19168.
- 184 A. Menichetti, D. Mordini and M. Montalti, *Nanomaterials*, 2024, **14**, 303.
- 185 F. Chen, Y. Xing, Z. Wang, X. Zheng, J. Zhang and K. Cai, *Langmuir*, 2016, **32**, 12119–12128.
- 186 C. J. Ochs, T. Hong, G. K. Such, J. Cui, A. Postma and F. Caruso, *Chem. Mater.*, 2011, **23**, 3141–3143.
- 187 B. Y. Guan, L. Yu and X. W. Lou, *J. Am. Chem. Soc.*, 2016, **138**, 11306–11311.
- 188 B. Y. Guan, S. L. Zhang and X. W. (David) Lou, *Angew. Chem.*, 2018, **130**, 6284–6288.
- 189 X. Wang, J. Zhang, H. Li, R. Zhang, X. Yang, W. Li, Z. Li, Z. Gu and Y. Li, *ACS Appl. Mater. Interfaces*, 2024, **16**, 22493–22503.
- 190 Z. Lu, A. M. Douek, A. M. Rozario, R. F. Tabor, J. Kaslin, B. Follink and B. M. Teo, *J. Mater. Chem. B*, 2020, **8**, 961–968.
- 191 H. Ma, J. Peng, J. Zhang, L. Pan, J. Ouyang, Z. Li, B. Guo, Z. Wang, Y. Xu, D. Lian and X. Zeng, *Pharmaceutics*, 2023, **15**, 15.
- 192 Z. He, H. Su, Y. Shen, W. Shi, X. Liu, Y. Liu, F. Zhang, Y. Zhang, Y. Sun and D. Ge, *RSC Adv.*, 2019, **9**, 9968–9982.
- 193 X. Liu, Z. Xie, W. Shi, Z. He, Y. Liu, H. Su, Y. Sun and D. Ge, *ACS Appl. Mater. Interfaces*, 2019, **11**, 19763–19773.



- 194 H. Hashemi-Moghaddam, S. Zavareh, E. M. Gazi and M. Jamili, *Mater. Sci. Eng., C*, 2018, **93**, 1036–1043.
- 195 L. B. Vong, Y. Sato, P. Chonpathompikunlert, S. Tanasawet, P. Hutamekalin and Y. Nagasaki, *Acta Biomater.*, 2020, **109**, 220–228.
- 196 S. Kang, R. Baskaran, B. Ozlu, E. Davaa, J. J. Kim, B. S. Shim and S. G. Yang, *Biomedicines*, 2020, **8**, 417.
- 197 P. Zheng, B. Ding, R. Shi, Z. Jiang, W. Xu, G. Li, J. Ding and X. Chen, *Adv. Mater.*, 2021, **33**, 2007426.
- 198 M. Nazemian, V. Hojati, S. Zavareh, H. Madanchi and H. Hashemi-Moghaddam, *Int. J. Pept. Res. Ther.*, 2020, **26**, 259–269.
- 199 H. Hashemi-Moghaddam, M. Ebrahimi, B. Johari and H. Madanchi, *J. Biomed. Mater. Res., Part B*, 2021, **109**, 1578–1587.
- 200 X. Zheng, J. Zhang, J. Wang, X. Qi, J. M. Rosenholm and K. Cai, *J. Phys. Chem. C*, 2015, **119**, 24512–24521.
- 201 Y. Li, C. Jiang, D. Zhang, Y. Wang, X. Ren, K. Ai, X. Chen and L. Lu, *Acta Biomater.*, 2017, **47**, 124–134.
- 202 M. Witkowska, E. Golusińska-Kardach, W. Golusiński and E. Florek, *Int. J. Mol. Sci.*, 2023, **24**, 4890.
- 203 Y. Liu, K. Ai, J. Liu, M. Deng, Y. He and L. Lu, *Adv. Mater.*, 2013, **25**, 1353–1359.
- 204 Y. H. You, Y. F. Lin, B. Nirosha, H. T. Chang and Y. F. Huang, *Nanotheranostics*, 2019, **3**, 266–283.
- 205 Y. Gao, X. Wu, L. Zhou, Y. Su and C. M. Dong, *Macromol. Rapid Commun.*, 2015, **36**, 916–922.
- 206 K. K. Lee, K. W. Park, S. C. Lee and C. S. Lee, *Theranostics*, 2025, **15**, 1077–1093.
- 207 X. Wan, C. Zhang, P. Lei, H. Wang, R. Chen, Q. Yang, Y. Cheng, W. Wu, D. Sun and X. Hong, *J. Mater. Chem. B*, 2025, **13**, 3245–3269.
- 208 S. Ren, X. Xiao, J. Lv, S. Lv, X. Wang, R. Liu and Q. X. Kong, *Front. Mater.*, 2024, **11**, 1396397.
- 209 T. Tarhan, A. Dündar, V. Okumuş and M. Çulha, *ChemistrySelect*, 2021, **6**, 4217–4223.
- 210 Z. Lu, S. Acter, B. M. Teo, A. I. Bishop, R. F. Tabor and M. L. P. Vidallon, *J. Mater. Chem. B*, 2022, **10**, 9662–9670.
- 211 G. Niu, L. Zhao, Y. Wang and Y. Jiang, *ChemPhysMater*, 2023, **2**, 83–89.
- 212 Y. Ding, S. Su, R. Zhang, L. Shao, Y. Zhang, B. Wang, Y. Li, L. Chen, Q. Yu, Y. Wu and G. Nie, *Biomaterials*, 2017, **113**, 243–252.
- 213 N. Wang, Y. Yang, X. Wang, X. Tian, W. Qin, X. Wang, J. Liang, H. Zhang and X. Leng, *ACS Biomater. Sci. Eng.*, 2019, **5**, 2330–2342.
- 214 L. C. Almeida, R. D. Correia, B. Palys, J. P. Correia and A. S. Viana, *Electrochim. Acta*, 2021, **386**, 138515.
- 215 L. C. Almeida, J. F. Zeferino, C. Branco, G. Squillaci, A. Morana, R. Santos, P. Ihalainen, L. Sobhana, J. P. Correia and A. S. Viana, *Bioelectrochemistry*, 2025, **161**, 108826.
- 216 G. Emilsson, K. Liu, F. Höök, L. Svensson, L. Rosengren, L. Lindfors and K. Sigfridsson, *ACS Nano*, 2023, **17**, 24725–24742.
- 217 M. A. Hudson, L. Sandoval, P. D. Susilo, D. Sim, M. B. Pena, S. Pizzo, D. Ezekoye, A. Maheshwari, S. Cho, R. Sharma, M. Lanchantin, S. Zale, G. Traverso, R. Langer, R. Dhanda and V. Sethuraman, *J. Endocr. Soc.*, 2025, **9**, 92–93.
- 218 J. Li, T. Wang, A. R. Kirtane, Y. Shi, A. Jones, Z. Moussa, A. Lopes, J. Collins, S. M. Tamang, K. Hess, R. Shakur, P. Karandikar, J. S. Lee, H. Huang, A. Hayward and G. Traverso, *Sci. Transl. Med.*, 2020, **12**, eabc0441.

